PEOPLE’S DEMOCRATIC REPUBLIC OF ALGERIA
MINISTRY OF HIGHER EDUCATION AND SCIENTIFIC RESEARCH

ABOU-BEKR BELKAID UNIVERSITY – TLEMCEN

THESIS

Presented to:

FACULTY OF SCIENCES – DEPARTMENT OF PHYSICS

In partial fulfillment of the requirements for the degree of:

MASTER IN PHYSICS

Specialization: Plasma Physics

By:

Ms. YOUBI Rihem

On the topic:

Supercontinuum Generation in water: Nonlinear Phenomena and Parameter Optimization

Publicly defended on 15/06/2025 in the presence of the jury composed of:

Dr Rerbal Benali	MCA	Tlemcen University	President
Pr. Zeyneb Bedrane	Prof	Tlemcen University	Supervisor
Dr. Amel Boutasta	MCA	Tlemcen University	Examiner

Academic Year: 2024–2025

Acknowledgements

First and foremost, all praise and gratitude are due to Allah, the One and Only, who granted me strength, clarity, and perseverance to accomplish this work. It is through His generosity and the gift of reason that we are able to seek knowledge and walk the path of learning. I pray that this work may be accepted sincerely for His sake and be a small contribution to the light of understanding.

My heartfelt thanks and deep appreciation go to my supervisor, Pr. Bedrane Zeyneb, for her unwavering support, insightful guidance, and dedication throughout this research. Her precision, passion for teaching and genuine encouragement have been invaluable. May Allah bless her and guide her steps...

I am also deeply grateful to the members of the defense jury: Dr. Rerbal Benali and Dr. Amel Boutasta, for accepting to evaluate my work and for their time and attention. I truly hope this modest contribution meets their expectations and adds value to this field of study.

My sincere thanks go as well to the Laboratory Team of Theoretical Physics Research, for granting us this opportunity and supporting us through access to resources and a stimulating academic environment.

Special thanks are also extended to the University of Abou Bekr Belkaid -Tlemcen- for providing a rich and inspiring academic journey. I would especially like to acknowledge Prof. Liani Bachir, Head of the Plasma Physics specialization, for his continued efforts in ensuring the quality of this formation. I sincerely hope we have met your expectations and honored the trust you placed in us.

Last but not least, heartfelt thanks to everyone who contributed, directly or indirectly, to the realization of this work...

May it serve as a useful reference for future generations and benefit all who read it.

Dedication

To the two souls who planted in me the love of giving, and wrapped my spirit in serenity...

To those who have always been my constant prayer, my answered wish...

To my parents, whose love strengthened my spine, and whose wisdom guided my steps; This work is yours token of endless love and eternal gratitude.

To my siblings,
Blessed am I with two sisters who are the very eyes through which I see the world, and two brothers, the arms that steadied me when I trembled. To you, I offer the fruit of my journey...

To my extended family,
May you hold pride in having your first graduate; This is for you.

To my kids, whom I have yet to meet,
Know that your mother walked this road with courage, stumbled yet rose, so that she may pass down to you a legacy of unyielding will, and a pride that time cannot dim.

To every soul who entered my life and lit a candle within it...

To my late friend Chifa,
You were, and will always remain, the silent prayer I whisper to God. I know you're witnessing this moment from a place far more radiant than here. Your light lives on through every success I reach.

And finally, to myself,
To the woman who stood alone when the lights went out...
Who gathered her pieces with bare hands and wiped her own tears unseen...
To the one who believed through the doubt, and fought through the fear...
This work is for you, for every night you wept in silence;
For every time you said "I will go on", and you did.
I am proud of you...
and I always will be.

"It always seems impossible until it's done."

— Nelson Mandela —

Contents

List of Figures

List of Tables

Liste of Abbreviations

CMOS: Complementary Metal-Oxide-Semiconductor

CRDS: Cavity Ring-Down Spectroscopy

DWDM: Dense Wavelength Division Multiplexing

e.m.: electromagnetic

FWHM: Full Width at Half Maximum

GNLSE: Generalized Nonlinear Schrodinger Equation

GVD: Group Velocity Dispersion

IBBCEAS: Incoherent Broad-Band Cavity-Enhanced Absorption Spectroscopy

IR: Infra-Red

IR-ATR: Infrared Attenuated Total Reflection

MID: Mid-Infrared

MPI: Multiphoton Ionization

Nd: YAG: Neodymium-doped: Yttrium Aluminum Garnet

NIR: near infra-red

NLO: Nonlinear Optics

OFC: Optical Frequency Comb

PCF: Photonic Crystal Fiber

PIE: Pulsed Interleaved Excitation

SC: Supercontinuum

SCG: Supercontinuum Generation

SF: Self-Focusing

SPM: Self Phase Modulation

UV: Ultraviolet

WDM: Wavelength Division Multiplexing

WLS: White Light Source

ZDW: Zero Dispersion Wavelength

Introduction

Introduction

The interaction of intense laser light with matter has long fascinated the scientific community, revealing a rich landscape for nonlinear optical phenomena. One of the most important among these is supercontinuum generation (SCG), the process in which a narrowband laser pulse is converted into a broad spectrum of light. SCG has enabled remarkable developments in several fields (e.g., spectroscopy, biomedical imaging, ultrafast science, and medicine). While it has been extensively studied in gaseous and liquid media, particularly water, due to its practical and scientific relevance.

Water represents a crucial and unique platform for nonlinear optical research. It is biocompatible, available, and transparent over a wide range of wavelengths, which makes it attractive for vital applications in biological, chemical, and environmental systems. Furthermore, its strong nonlinear refractive index allows for the exploration of light-matter interaction.

This study is devoted to the numerical exploration of SCG in water using femtosecond laser pulses. By solving the Generalized Nonlinear Schrodinger Equation (GNLSE), and simulating the evolution of the laser pulse and the resulting spectrum, we can respond to the central problem of the study:

What are the global effects that lead to supercontinuum generation in water?

What are the optimal physical conditions that allow efficient and stable supercontinuum generation in water when using a femtosecond laser pulse?

The goal of this study is to gain a deeper understanding of the mechanisms underlying supercontinuum generation (SCG) in water when excited by femtosecond laser pulses, with a specific focus on identifying and optimizing the nonlinear parameters that maximize spectral broadening.

The structure of this thesis is as follows:

Chapter I: introduces the fundamentals of supercontinuum generation and outlines its historical development and main applications.

Chapter II: discusses the nonlinear optical effects relevant to SCG in transparent media, with a particular focus on femtosecond interactions in water.

Chapter III: describes the theoretical modeling approach, including the derivation of the GNLSE and the numerical methods employed.

Chapter IV presents the simulation results and a comprehensive discussion of the key mechanisms and trends observed.

Finally, the Conclusion summarizes the main findings and offers perspectives for future work, both theoretical and experimental.

By combining nonlinear theory with numerical modeling, this thesis aims to bridge the gap between experimental observations and theoretical predictions of SCG in water. The insights gained here contribute not only to a deeper understanding of light-matter interaction in liquids but also to the development of practical strategies for optimizing supercontinuum sources in aqueous environments.

Supercontinuum and its Applications

I. Supercontinuum and its Applications

I.1 Definition and Evolution of supercontinuum

The supercontinuum refers to an extremely broad spectrum of light spanning visible to mid-infrared wavelengths, originating from non-linear optical effects. It has many strong characteristics, such as high coherence, ultra fast pulse duration, and tunable wavelengths for adaptable applications[1](shown in Fig. I.1). Today, supercontinuum light is widely used in a range of fields such as spectroscopy, biomedical diagnostics, telecommunications, etc.

Singh and Ravindra[2] present the supercontinuum as a nonlinear optical process in which dramatic spectral broadening of intense picosecond or femtosecond laser pulses occurs as they propagate through the nonlinear medium (condensed (solid) or gaseous). This spectral broadening develops thanks to the combined action of various nonlinear optical effects.

Troung X[3] and his team believe that supercontinuum generation (SCG) is one of the most important phenomena in nonlinear optics, widely used in various applications. It involves the rapid and extensive spectral broadening of a short, intense laser pulse as it propagates through a nonlinear medium.

The SCG phenomenon began to take shape in the late 1960s, after the invention of the laser, especially in 1963, Stoicheff [4] focused a high-intensity ruby laser beam into various transparent liquids and observed that the light scattered from the medium contained new frequencies, Stokes lines (longer wavelengths) corresponding to the vibrational modes of the liquid's molecules. This experiment proved that the Raman effect could be stimulated, meaning that the optical response was strongly enhanced by the laser intensity.

In 1970, Alfano and Shapiro [5] realized the first experiment to observe the birth of SCG by focusing intense picosecond pulses at 5300 Å into glass, observing a broadband emission spanning from 4000 Å to 7000 Å far beyond the original wavelength of the laser. This experiment demonstrated how intense ultrashort laser pulses could interact with a transparent medium and create a special spectrum. This phenomenon was called “white-light generation”.

After this study, many researchers began investigating this phenomenon in various transparent solids and liquids.

In 1978, Lin and Nguyen [6] published a crucial study in which they used a high-energy pulse of light set to a 1064 nm wavelength (Infrared region). They tested two types of fibers: multi-mode and single-mode doped with GeO_2 (Germanium Dioxide) to enhance the nonlinear optical properties. After coupling the laser light into the fiber, the generated laser pulse caused nonlinear interactions within the fiber and thus made it spread out into a broad spectrum. The spectrum of the output light ranged from the visible to the near Infrared region, and they observed that when they increased the input power beyond 50 kW, the spectrum extended further, even into the green part of the visible spectrum. At these higher powers, the fiber was damaged, leading to the conclusion that it's very important to carefully control the power coupled into the fiber to avoid damage and obtain the optimal results [6].

In 1980, Fujii et al. [7] continued Lin's experiment by using a mode-locked Nd:YAG laser to generate shorter pulses with higher peak powers (> 100 kW), in a 10 μm core, single-mode Ge-doped silica fiber. The resulting spectrum extended from 300 nm (UV) to 2100 nm (IR), and they also observed higher-order modes due to sum-frequency generation between the core and the cladding modes. This study showed that the SC spectrum could range into both UV and IR regions, opening new thinking about fiber design for enhanced results.

In the same year, Washio and his team [8] pumped a 150 m length of single-mode fiber using a Q-switched Nd: YAG laser at 1.34 μm, which is in the anomalous dispersion regime of silica. They generated a continuum from 1.15 to 1.6 μm without discrete Stokes lines. At this point, no one had really explained why the spectrum was smooth between Stokes lines at longer wavelength in the fibers. This smoothness was one of the signs of the SCG as a result of dispersion management.

In 1991, Gross and his team [9] published a comprehensive theoretical model for SCG in the anomalous dispersion regime, based on the progress of Self-phase modulation developed in the late 1980s, using femtosecond pulses in optical fibers. This was the most complete model to that date, introducing the concept of the soliton self-frequency shifts (the redshift of the soliton due to intrapulse Raman scattering). This model became a fundamental base for understanding femtosecond SCG.

In 1993, Morioka et al.[10] explored how SCG could serve in optical telecommunications by creating a 100-channel wavelength-division multiplexing (WDM) system, generating 100 simultaneous 10 ps pulses across the 1.224 to 1.394 μm range. It marked the first practical application of SC light in telecom systems.

By the late 1990s, researchers had established that pumping in the anomalous dispersion regime leads to spectrum broadening. In the 2000s, Ranka et al. used a short length of photonic crystal fiber (PCF), which is a newer type of fiber with microstructured cladding, enabling for tailored dispersion properties and enhanced nonlinearity. They pumped with 790 nm pump wavelength, placed near ZDW, which allowed the formation of high-order solitons and generation of dispersive wave which contributed in the broadening. The resulting SC extended from 400 nm (V violet) to 1450 nm (NIR). This was the first time that a femtosecond laser was combined with a PCF to generate an ultra-broad spectrum, which is the supercontinuum[11], [12], [13]. These studies on SCG created a crucial foundation for many technological uses. Thanks to the development of new laser sources, SCG became a powerful tool. This opened the door to a wide range of essential applications in many fields, such as telecommunication, biology, medicine...

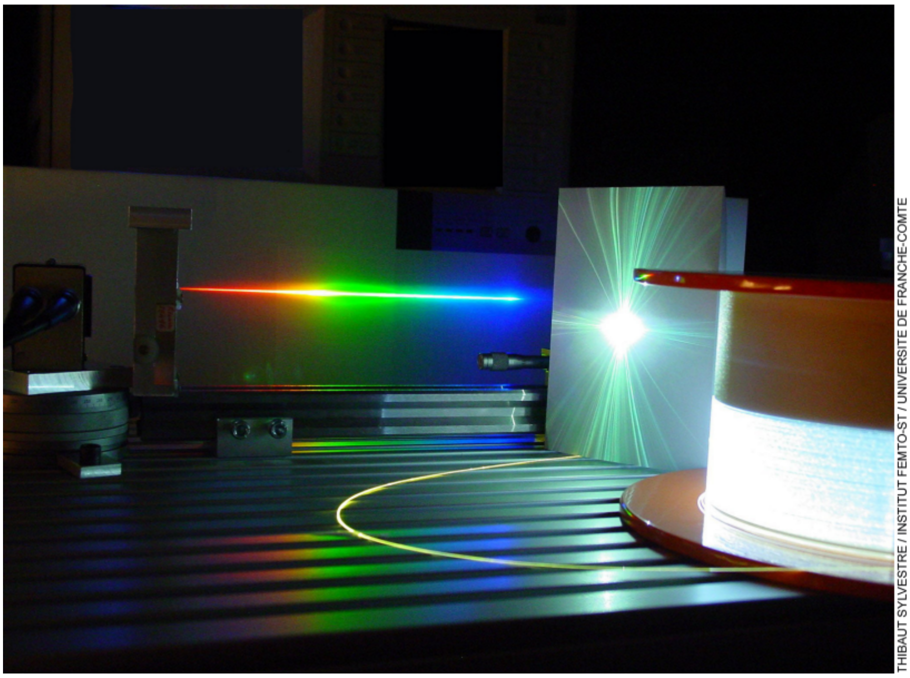

Figure I.1: **White-light supercontinuum generation, generated by injection of a femtosecond laser (800 nm) into a long photonic crystal fiber (50 m).** [14]

I.2 Applications of supercontinuum

I.2.1 Spectroscopy

- **Absorption spectroscopy**

  When the supercontinuum is used in absorption spectroscopy, it significantly enhances measurements compared to traditional narrow band or incoherent sources like LEDs or arc lamps. Thanks to its wide range of wavelengths, SC enables concurrent multi-wavelength absorption measurements. Due to its higher intensity, SC in absorption spectroscopy improves the signal-to-noise ratio and enhances sensitivity for detecting low-concentration traces. In the study of [15] about Incoherent Broad-Band Cavity-Enhanced Absorption Spectroscopy of azulene in a supersonic jet, the authors compared the spectrum of Cavity Ring-Down Spectroscopy (CRDS), which is based on a traditional narrowband tunable laser, with Incoherent Broad-Band Cavity-Enhanced Absorption Spectroscopy (IBBCEAS), which relies on a broad-band source like SC light. The result is shown in Fig I.2 [15].

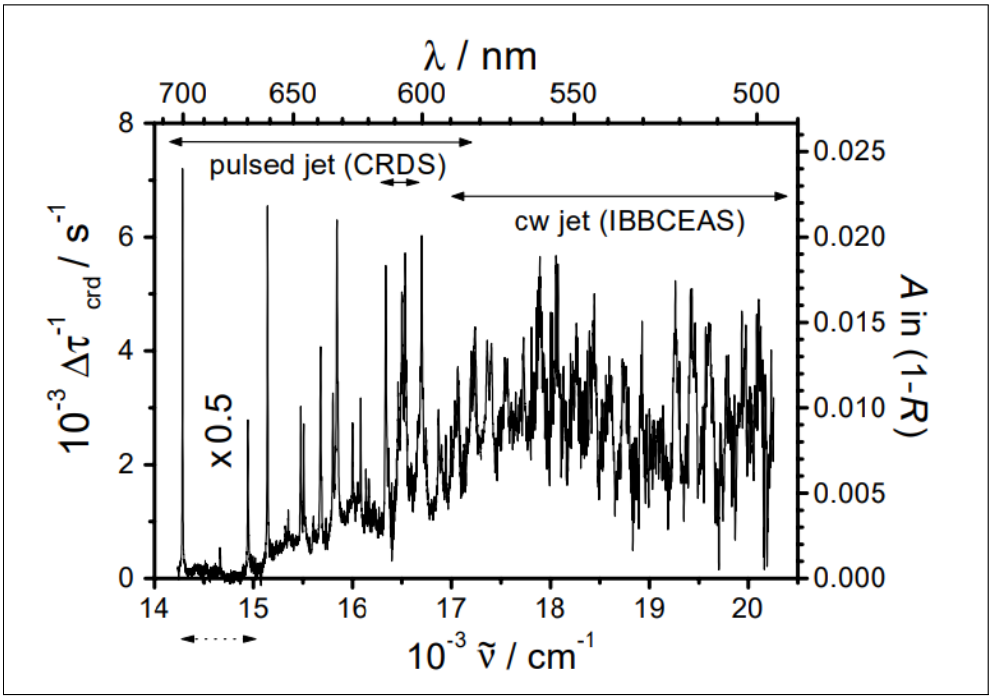

Figure I.2: **Comparison of Absorption Spectra: CRDS vs IBBCEAS for $S_1 \leftarrow S_0$ absorption spectrum of jet-cooled azulene measured with CRDS (left axis) and IBBCEAS (right axis)** [15]

Unlike the CRDS process, which provides information at specific wavelengths, the IBBCEAS process delivers a continuous absorption spectrum, revealing more spectral details. This makes SC light a powerful source for broadband, high-resolution spectroscopic applications.

- **Fluorescence spectroscopy**

  The supercontinuum laser emits a broad spectrum of light, allowing various choices of excitation of different fluorophore wavelengths from one source. Due to picosecond pulses, the pulsed interleaved excitation (PIE) will be smoother and easier because distinct fluorophores are excited at the same moments, reducing the spectral overlap and improving the precision of fluorescence measurements. Also, the use of one source makes the optical setup simpler and adaptable to various experimental conditions. This type of spectroscopy (PIE), using supercontinuum source, is used for various applications such as studying protein interactions, molecular dynamics, medical diagnostics, Etc. The figure I.3 illustrates the application of fluorescence spectroscopy in plant tissue, specifically in plant *convallaria majalis*, or lily of the valley. The image in (a) represents the excitation of fluorescence emission at 620 nm, and (b) corresponds to excitation at 513 nm, (c) is the plot that displays Fluorescence emission spectra for four different regions mentioned in (a). The use of a supercontinuum light source in fluorescence spectroscopy enhances the broadening of the spectrum, improving the ability to analyze different biochemical compositions of plant tissue, which provides information on cellular structure, metabolic change, ...etc[16].

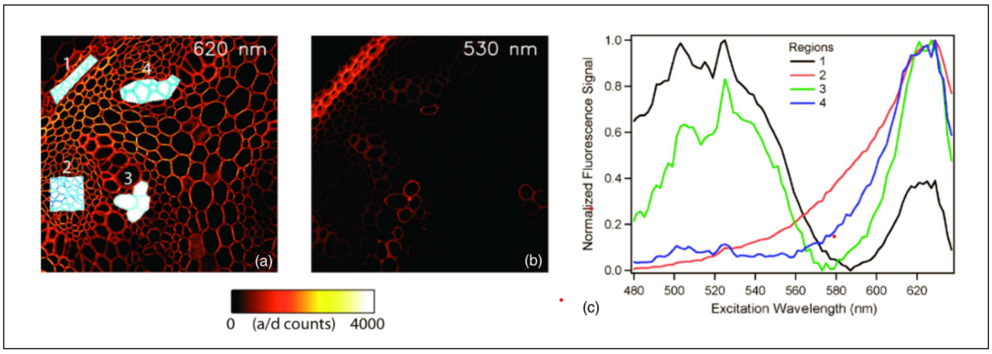

Figure I.3: **Spatial variations in fluorescence emission under different wavelengths (530 nm and 620 nm) for plant tissue (*Convallaria majalis*)** [16].

I.2.2 Biomedical and clinical diagnostics

- **Miniaturized endoscopes**

  The SC boosts the broadening of the spectrum, which is integrated into a miniaturized endoscopic system for in vivo imaging of biological tissues, in Figure I.4, specifically using ”nude mice”. When the SC is generated, it’s first collimated to make the beam parallel, facilitating smoother coupling into the fiber. After that, it passes through an IR filter to eliminate unwanted infrared elements to avoid damage to tissues. The optical filter chooses the best wavelength range for the specific excitation of biomolecules. The multi-mode Fiber patch cable transmits the high-intensity light to the sample, which is then diffused through a diffusion tip, enhancing uniform illumination of the tissue by broadening the illumination angle from 10 degrees to over 80 degrees, the signal emitted after excitation is captured by the miniature CMOS camera, permitting the detection of metabolic changes, tumor, biological dynamics... etc. The color checker is used as a reference to calibrate the color rendering index and compare the quality of light with traditional sources [17].

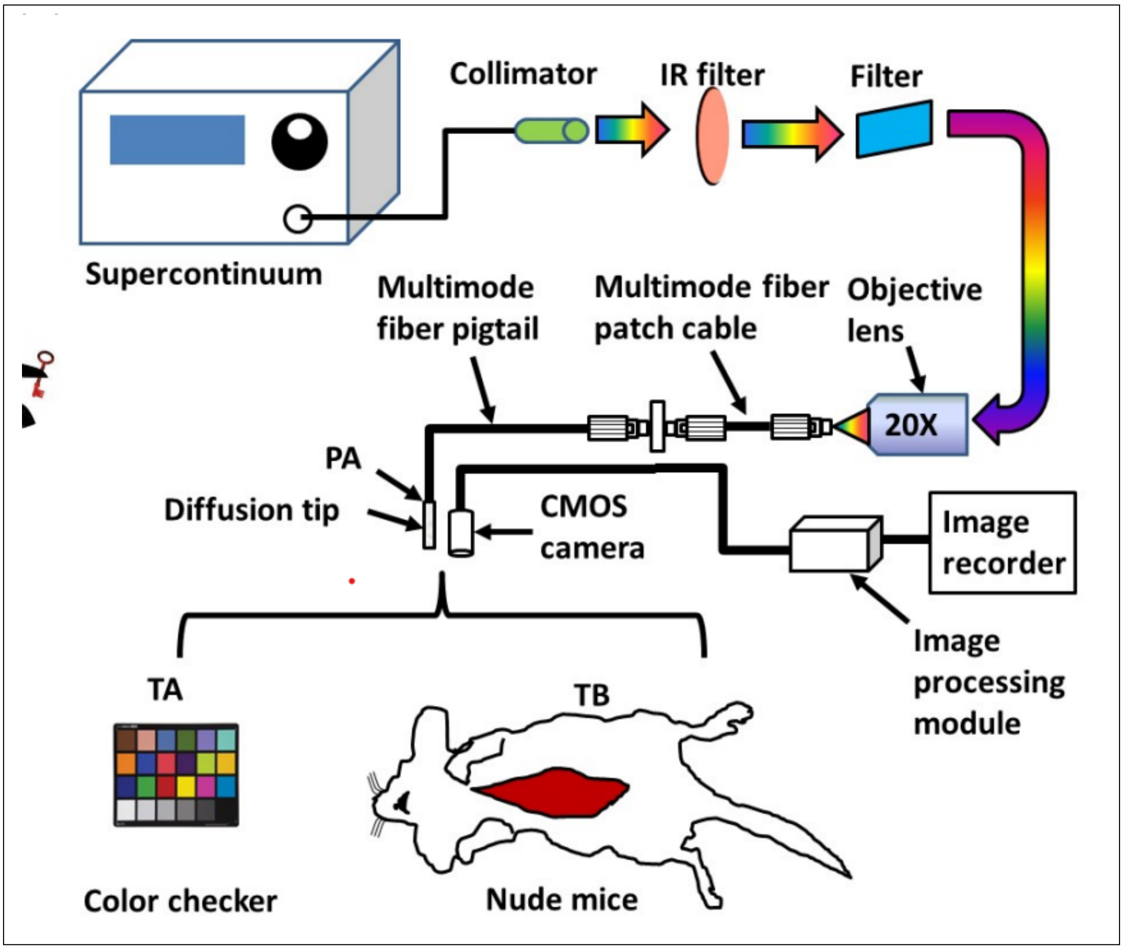

Figure I.4: **The schematic setup of SC light through a fiber coupling. TB represents the biological tissue of the "nude mice" used for imaging analysis; TA is the color checker used for light calibration [17].**

As illustrated in Figure I.5, the supercontinuum with the diffuser and short pass filter offers the best uniform illumination with accurate color representation for this application [17].

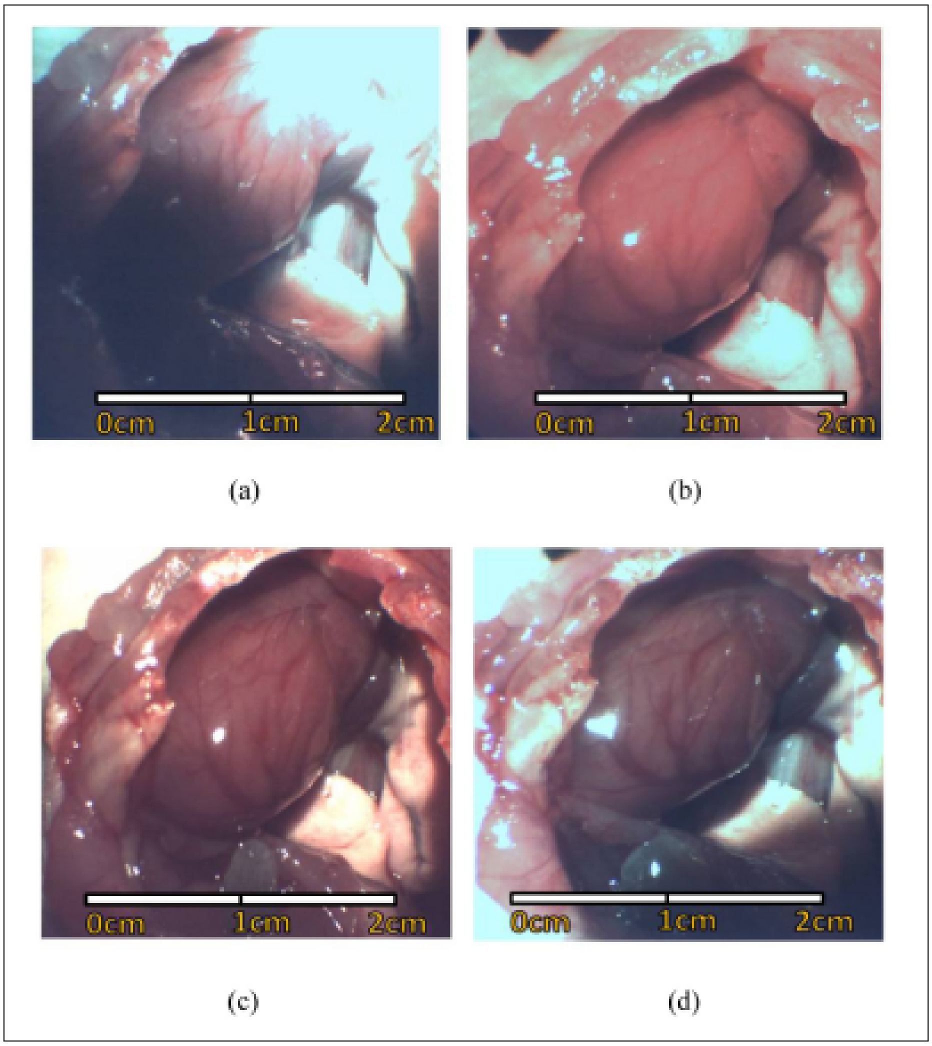

Figure I.5: **The images of CMOS camera with the previous setup; (a) the thoracic cavity of nude mice illuminated by SC without diffuser; (b) SC with diffuser and without filter; (c) SC with diffuser and filter, (d) white LED** [17].

I.2.3 Telecommunication

- **Optical fiber** is a technology that uses light signals to transmit data through optical fibers made of glass or plastic. This process permits high-speed data transmission over long distances with minimal loss. It's widely used for internet traffic, telecommunication, LANs (local area networks), cable TV, etc[18].

  Optical Frequency Combs (OFCs):

  An optical frequency comb is a broad spectrum composed of discrete spaced lines, which are generated by mode-locked lasers (MLLs) that emit a range of ultrashort pulses, enabling the transmission of data across numerous channels. This efficiency enhances the data carrying capacity of optical networks facilitating communication systems. The role of supercontinuum in OFCs is to offer a broad spectrum that can be optimized into a frequency comb, allowing the creation of ultra-broadband sources, that is essential for Dense Wavelength Division Multiplexing (DWDM) systems, as shown in Figure I.6 [19].

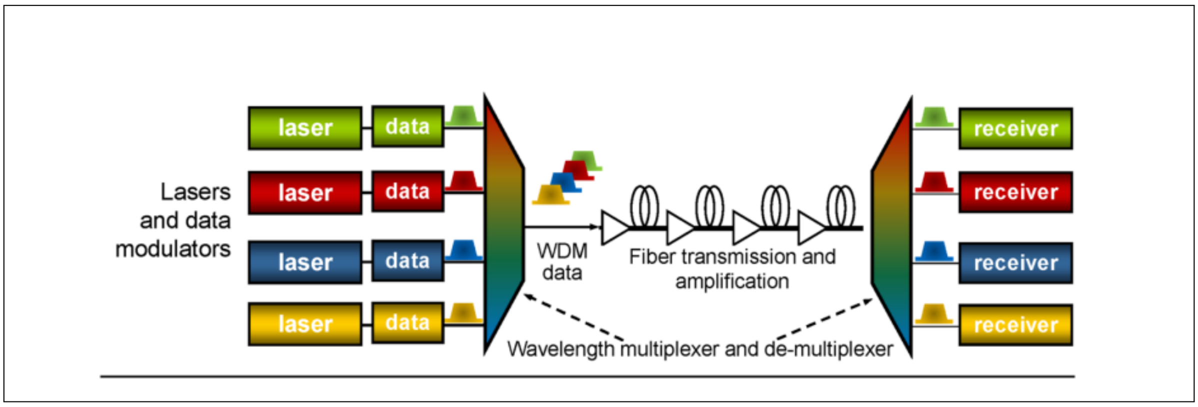

Figure I.6: **Optical communication system with wavelength multiplexer and de-multiplexer channels [19].**

Different lasers with different wavelengths are modulated with the data signal, which is combined into a single fiber using a wavelength multiplexer. This signal is amplified along its travel through an optical fiber. At the end, the de-multiplexer separates the received signal again and captures it by specific receivers. The power of the OFC process is to replace the traditional WDM (multiple lasers) with this comb structure (hundreds of frequencies from the SC spectrum), enabling more stable data transmission in optical communications.

In this chapter, we investigated different fields of supercontinuum applications, from its crucial role in absorption and fluorescence spectroscopy to its influence on medical and biological diagnostics through diverse examples of tissues. Finally, its significant advancement in telecommunication through Optical Frequency Combs. These various applications highlight the SC's importance in precision, data transmission capacity, and 3D resolution, opening the door to a bright future with brilliant innovations in diverse fields of development.

Supercontinuum Generation in Water: Dominant Nonlinear Processes

II. Supercontinuum Generation in Water: Dominant Nonlinear Processes

The supercontinuum generation (SCG) has advanced several areas of scientific and technological research thanks to its unique ability to transform a narrowband laser pulse into a vast broad spectrum (rainbow of light) with high intensity and coherence. This process is based on various nonlinear effects, which are the key to SCG. In this chapter, we focus on the physical principles underlying SCG in water, where these nonlinear effects play a fundamental role in the resulting spectral broadening.

II.1 Nonlinear phenomena in SCG in water

Supercontinuum generation (SCG) is essentially driven by diverse nonlinear phenomena that interact with the light source (intense laser pulse) as it spreads through a medium, producing spectral broadening. In water, only specific subgroups of these nonlinear phenomena dominate due to its unique properties.

II.1.1 Kerr effect

Nonlinear optics (NLO) is the study of the interaction between intense light (femtosecond or picosecond laser) and matter when the response of the medium is dependent on the applied electric field. Unlike linear optics, where light propagates without changing the medium's fundamental properties, nonlinear optical effects occur when the beam intensity is strong enough to modify the medium's properties. With the birth of this term (NLO) came the emergence of Kerr effects [20].

In 1875, Kerr John observed that the isotropic materials change their behavior in the presence of a strong electric field becoming anisotropic, the refractive index depends on the direction of an electric field, inducing birefringence phenomenon (double refraction), leading to the transformation of laser pulses' polarization state from linear to elliptical shown in figure II.1 [21]. The polarization P is given by:

$$P = \chi^{(1)}E + \chi^{(2)}E^2 + \chi^{(3)}E^3 + \dots \tag{II.1}$$

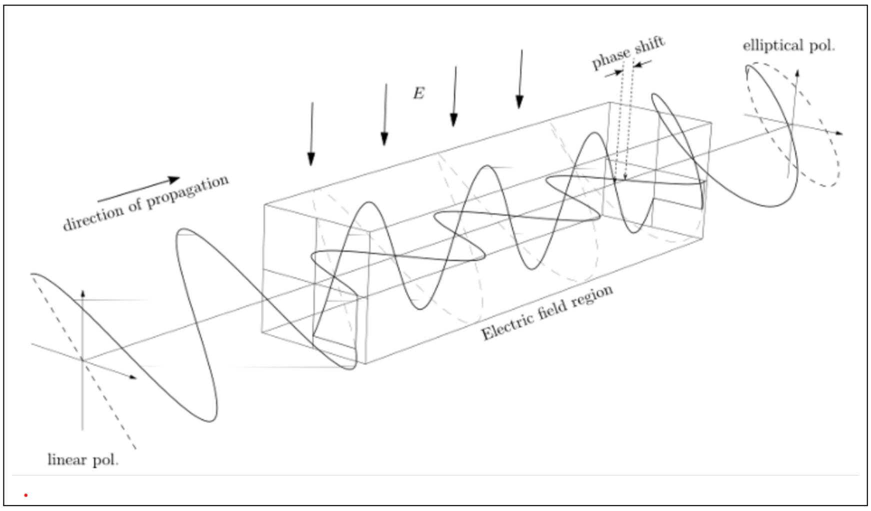

Figure II.1: **the schematic representation of the Kerr effect [21].**

Due to the Kerr effect, high optical intensity in the medium causes a nonlinear phase shift as the light source propagates. In simple terms, the Kerr effect is described as a change in the refractive index in an intensity-dependent manner [22]:

$$\Delta n = n_2 \cdot I \tag{II.2}$$

With:

- Δn: The change in the refractive index due to the Kerr effect.
- n_2: The positive nonlinear refractive index coefficient.
- I: The optical intensity of the incident light.

II.1.2 Self Phase Modulation (SPM)

Self-phase modulation is a nonlinear phase modulation of the light beam caused by its intensity when it passes through a nonlinear medium. This phenomenon is caused by the Kerr effect, inducing a time dependent phase shift in optical pulses[23], forming new frequencies in the spectrum. The evolution of the temporal phase is given by [24]:

$$\omega(t) = -\frac{\partial \phi}{\partial t} \sim \omega_0 - \frac{n_2 \omega_0}{c} z \frac{\partial I(r,t)}{\partial t}. \tag{II.3}$$

Where:

- $\omega(t)$: Time-evolution of the instantaneous angular frequency of the optical field.
- ϕ: Optical field's phase.
- t: Time.
- n_2: Nonlinear refractive index coefficient (positive).
- c: The speed of light.
- z: Propagation distance in Kerr medium.
- $I(r,t)$: Optical intensity (function of distance r and time t).
- $\frac{\partial I(r,t)}{\partial t}$: Temporal derivative of the intensity

The generation of new frequencies depends on the temporal derivative of the intensity, the distance z in the nonlinear medium, and its positive coefficient n_2. In a Kerr medium, the redder frequencies (longer-wavelength) are generated by the front of the beam because of its high intensity and high refractive index, and the back part bluer frequencies (shorter-wavelength) due to its lower intensity and refractive index [24].

II.1.3 Self Focusing (SF)

Self-focusing is a very complex phenomenon because it originates from the combination of various nonlinear effects occurring during the propagation of light (an intense laser pulse) through a nonlinear medium (refractive index depends on intensity). The core of this process is the optical Kerr effect, where the refractive index increases with the intensity, shaping the beam into a Gaussian profile (Figure II.2) [25], leading to self-induced lensing, causing the beam to shrink inward and become more intense, like a convex lens [25], when the pulse power exceeds the self-focusing threshold. The critical power for this process is (II.4) [26]:

$$P_{\mathrm{cr}} \approx \frac{3.77\lambda^2}{8\pi n_0 n_2} \tag{II.4}$$

Where: λ: The laser wavelength.

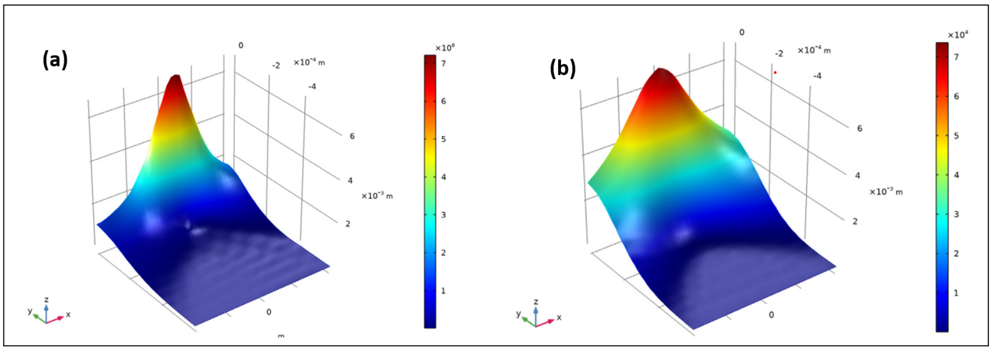

Figure II.2: **3D surface plots of spatial intensity evolution of a Gaussian beam. (a): represents the plot of a beam with high peak intensity. The center of the beam has a higher intensity than the edges, undergoing the self-focusing process, which makes the energy concentrate at the center. (b): represents the plot of a beam with low peak intensity. The intensity distribution is smoother, with a moderately low peak at the center, and the broad shape does not have a significant modification [25].**

II.1.4 Filamentation

Laser-pulse filamentation is a crucial branch of optical physics that studies laser matter, driven by varietal mechanisms. It happens when an intense, ultrashort laser pulse propagates through a nonlinear medium (Kerr medium), due to the dynamic balance between Kerr self-focusing (the intensity-dependent refractive index) and plasma-defocusing (caused by the strong electric field of the incident beam, ionizing the region around it creating plasma, which has a lower refractive index than the medium). This balance creates a narrow, constantly high-intensity channel that propagates over long distances, known as a “filament”, shown in Figure II.3. This process enriches the frequency-angular spectrum of the laser, leading to SCG [27].

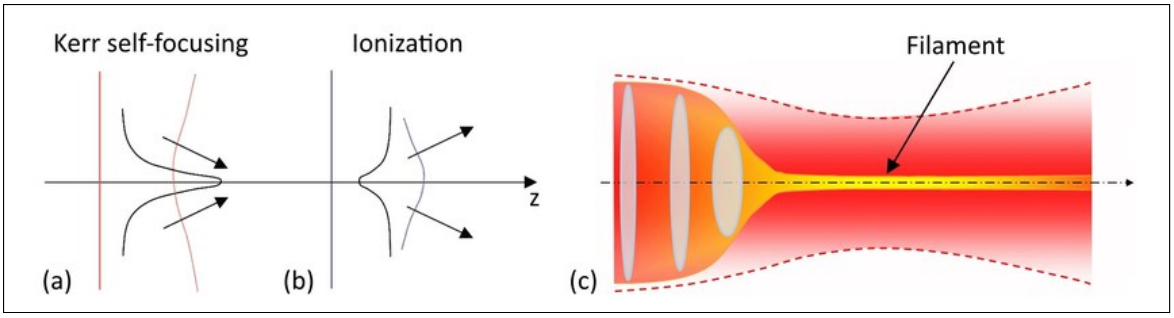

Figure II.3: **Schematic illustration of the laser filamentation process. (a) Kerr self-focusing of a beam. (b) Plasma defocusing of the beam. (c) Illustration of the beam shrinking and the creation of plasma that leads the beam out of this region, creating a long filament [28].**

II.1.5 Raman effect

The Raman effect is the study of light's interaction with the vibrational and rotational modes of molecules in inelastic scattering, using visible light. When laser pulses interact with the medium, they can excite these molecules to vibrational or rotational states, leading to Stokes or anti-Stokes shifts (depending on the energy of the scattered photons ”lower or higher than the incident photons”) [6] shown in Fig II.4 [6].

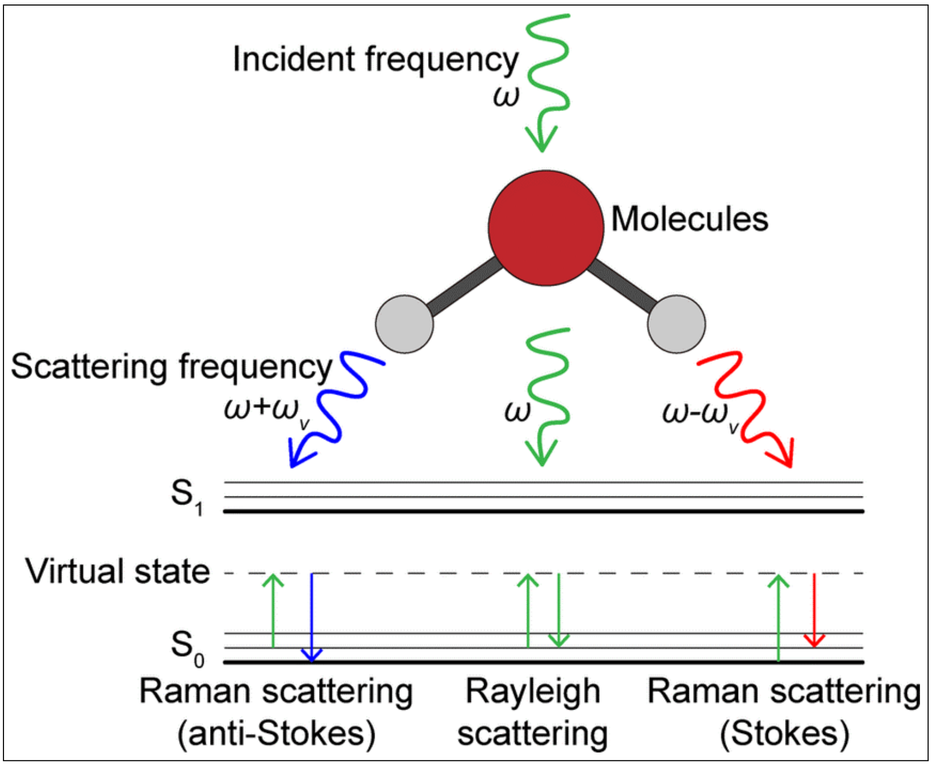

Figure II.4: **Illustration schematic of energy levels in Raman effect for molecular systems [6].**

- **Stokes**: When the energy of the incident light is higher than that of the scattered light. It occurs when the molecules of the incident photons absorb a photon and remain at a higher vibrational level, resulting in a scattered photon with lower energy. (see Fig II.4)
- **Anti-Stokes**: when the energy of the scattered light is higher than the incident light. It happens when the molecules are already in an excited vibrational state and absorb a photon, relaxing to a lower vibrational state, emitting a photon with higher energy. (see Fig II.4)
- **Rayleigh scattering**: When the energy of the scattered photon is the same as the incident photon. The initial and final vibrational states of the molecules are also the same, resulting in elastic scattering. (see Fig II.4)

The energy change in laser-medium interaction corresponds to the creation or destruction of a phonon (Stokes or anti-Stokes scattering), according to [29]:

$$\hbar\omega_s = \hbar\omega_i \mp \hbar\omega_p, \tag{II.5}$$

Where: $\hbar$: The reduced Planck constant. ω_i, ω_s, ω_p: are the frequency of the incident photon, the scattered photon, and the phonon, respectively.

n(w,t): The population factor of phonons at thermal equilibrium, given by [29]:

$$n(\omega, T) = \frac{1}{\exp\left(\frac{\hbar\omega}{k_B T}\right) - 1}, \tag{II.6}$$

Where:

- k_B: Boltzmann constant.
- T: Absolute temperature

The intensity of the scattered phonon is given by [29]:

$$I_s \propto I\chi''(\omega)\omega_s^3 \left\{ \frac{n(\omega, T) + 1}{n(\omega, T)} \right\}, \tag{II.7}$$

Where: $\chi''(\omega)$: The nonlinear susceptibility's imaginary part.

The Contribution of the Raman effect in supercontinuum generation (SCG) lies in the broadening of the spectrum. Stokes scattering generates red-shifted photons in the SC spectrum, enhancing the spectrum at long wavelengths (toward the infrared) [30].

Anti-Stokes scattering creates blue-shifted components, which are generally weaker than the red ones because they require a higher initial thermal excitation. They contribute to the SCG spectrum by adding short-wavelength (UV or Visible) photons [31].

In this chapter, we explore the fundamental nonlinear processes in SCG in water, focusing on its keys mechanisms, such as Kerr effect, self-phase modulation, self-focusing, filamentation, and Raman scattering, discussing the role of each in SCG. Clarifying these pieces of information for the best understanding and a simple vision of the whole phenomenon.

Interaction Medium and Source: Water and Laser Traits

III. Interaction Medium and Source: Water and Laser Traits

Supercontinuum generation in water results from a complex combination of vital nonlinear optical effects. Building upon these key aspects discussed in the previous chapter, in this one, it's essential to shift our focus to other parameters that influence this process. A deep understanding of the medium's properties (optical and physical) is fundamental for predictive modeling of ultrashort pulse propagation in such a medium.

III.1 Properties of water

Water is a ubiquitous and essential substance, it's marked as a highly relevant medium in the context of nonlinear optics. It has unique physical and optical properties that make it a promising candidate for various laser applications. Here are the most fundamental properties:

III.1.1 Dielectric nature

Water is a dielectric medium, which means it doesn't conduct electricity, but responds to an electric field by becoming polarized. It has vital properties, such as high relative permittivity. Because of its molecular polarity and hydrogen-bonding network, water can reduce the electric field within it. Its relative permittivity (ϵ_r) is estimated at 78.4 under room temperature conditions (25°C). Its behavior also depends on the frequency, at low frequencies, the permittivity is high because the molecular dipoles can follow the field of oscillations. However, the permittivity decreases at high frequencies, causing the dipoles to lag. At this condition of temperature, the relaxation time of water is 8.21 ps. Under high-intensity fields, the dielectric medium "water" exhibits a nonlinear response. These dielectric characteristics enable key nonlinear optical phenomena as SPM, SF, etc, which are the main processes of this study[32].

III.1.2 High refractive index n_2

The nonlinear refractive index n_2 is a parameter that quantifies the intensity-dependent change in the refractive index of a nonlinear medium. The searches prove that water has a high n_2 compared to many transparent dielectrics, enabling strong nonlinear interactions even at slight intensities [33].

In the newest study of Betka [34] on nonlinear optical refractive index measurements of pure water via Z-scan technique at 800 nm, the nonlinear refractive index was measured as $n_2 = (8 \pm 1.4) \times 10^{-20}$ m^2/W at 800 nm (NIR region) for pure water. These measurements are significant for understanding this property of water as a nonlinear medium for SCG application.

III.1.3 Absorption and transparency

Water absorption refers to the process by which water molecules take up electromagnetic radiation and relay it to other forms of energy [35]. It is a wavelength-dependent process that is influenced by molecular rotation, vibration, and electronic transition. Hale and Querry [36] demonstrate that water is almost transparent in the visible and NIR regions, making it ideal for transmitting high-intensity ultrafast pulses, enabling perfect propagation of laser without absorption losses. This transparency is essential for nonlinear phenomena like self-phase modulation, self-focusing, etc, and the longer interaction lengths allow more efficient spectral broadening in SCG [37, 36]. However, in the UV and MIR regions, water represents strong absorption bands; These absorption peaks arise firstly due to combination bands of vibrational modes in the MIR and electronic transitions in the UV [36].

At high intensities, the absorption in water can lead to an increase in temperature at the focal point, leading to ionization of water, which forms plasma, that can affect the generation of supercontinuum. As the plasma has a different refractive index than the water surrounding, which perturbs the phase matching conditions for wave propagation, reducing the spectral broadening. Additionally, the defocusing effect of the plasma causes the beam to diverge, reducing the intensity of the pulses at the focal point and thereby reducing the nonlinear interactions required for SCG [37, 38].

III.1.4 Dispersion characteristic

In optics, dispersion is the phenomenon describing the dependence of a wave's phase velocity on its frequency. This variation causes various wavelengths to propagate at different speeds through a medium, resulting in the separation of the light pulses into spectral components [39].

There are many types of dispersion. Normal dispersion is the decrease of the refractive index with the increasing wavelength, which makes the lower frequencies (redshifted) travel faster than the higher ones (blueshifted). When the refractive index increases with the wavelength, the dispersion is called anomalous, making the higher frequencies move faster [40]. Chromatic dispersion includes both normal and anomalous dispersion [41]. In water, all of these types can appear:

Normal dispersion: The water exhibits this type of dispersion in the visible range (400-700 nm). In the study of Daimon, M. et al. [42], they marked different refractive indices at various temperatures (Fig. III.1). In the results, the refractive index decreases as the wavelength increases, which proves the presence of normal dispersion in the near-infrared to the ultraviolet regions.

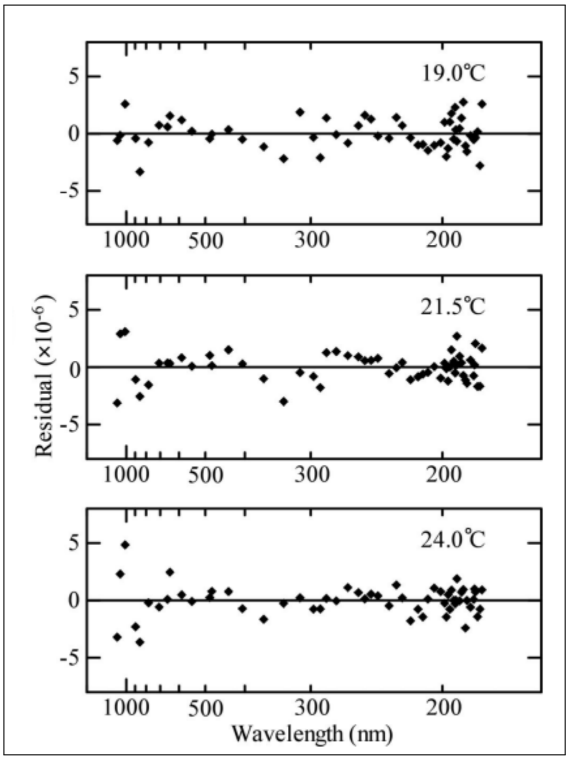

Figure III.1: **Wavelength dependence of fit residuals ($\times 10^{-6}$) for refractive index measured in water at different temperatures.** [42]

Anomalous dispersion: is widely observed in the ultraviolet (UV) and mid-infrared (MIR) regions near vibrational absorption bands [43], which is proven in the study of Mehmet Hancer and his team [44]. They used the Infrared Attenuated Total Reflection (IR-ATR) technique in which the IR beam is directed into a high refractive index crystal with an angle exceeding the critical angle of internal reflection [45], to test the optical behavior of the water in the MIR region. The comparison between the distortion near the strong vibrational absorption bands and the theoretical models confirmed that anomalous dispersion occurs in water exactly in this region (MIR), because of the rapid change of the refractive index with wavelength around the vibrational bands, which is the signature of anomalous dispersion [44]. In addition, in the UV regions, the researchers confirmed the presence of anomalous dispersion in the water.

Chromatic dispersion: is the most famous type of dispersion; it means that both normal and anomalous dispersion can appear in the same medium. In the search of Guoqiang Lan and his team [46], they used the liquid-prism SPR sensor setup, in which the incident light is focused on the metal layer placed on the prism. The SPR sensor detects changes in the refractive index of the medium, using a wide spectral range (from 450 to 1050 nm) at a temperature of 20°C. They observed that at short wavelengths the refractive index is high, and vice versa. This variation confirms that the refractive index varies across the spectrum, demonstrating that water exhibits chromatic dispersion. This study proposed a new practical application to measure the chromatic dispersion in liquids[46].

III.2 Laser characteristics

Lasers play a central role in generating a supercontinuum, as all of the nonlinear phenomena involved depend on the characteristics of the incident pulses, which are:

III.2.1 Pulse width and peak power

Pulse width refers to the duration of time a laser pulse occurs. The shorter pulses, typically from femtoseconds to picoseconds, generate higher intensities for such wavelengths (inversely proportional, Eq. III.1), which optimize nonlinear effects[47, 48]

$$P_{\text{peak}} = \frac{E}{\tau} \tag{III.1}$$

Where:

- E: The energy of the beam.
- τ: The duration.

Short pulses are capable of delivering extremely high peak powers even with moderate energy levels. This high peak intensity is critical for triggering various nonlinear optical effects such as SPM, self-focusing, Raman scattering, all of which contribute to SCG in water. [47, 48]

III.2.2 Wavelength

The choice of laser wavelength is a crucial step in each study, because it influences the light-medium interaction. For example, at (700 to 1300 nm, infrared regions), water exhibits low linear absorption, making the pulses propagate without any energy loss. This transparency is ideal for the nonlinear interactions, which are essential in various applications, such as in supercontinuum generation[49].

III.2.3 Monochromaticity

Refers to light emission with a single frequency or a very narrow range of wavelengths. This can occur with two processes: the first is the selective amplification, meaning that only electromagnetic (e.m.) waves of specific frequency can be amplified; the second process is the filtering of the resonance cavity, due to the mirrors of the optical resonator acting as a frequency-selective cavity that selects only certain modes, resulting in the oscillation occur only at those resonance frequencies (Fig III.2). This produces a narrower beam than the natural linewidth of the spontaneous emission.

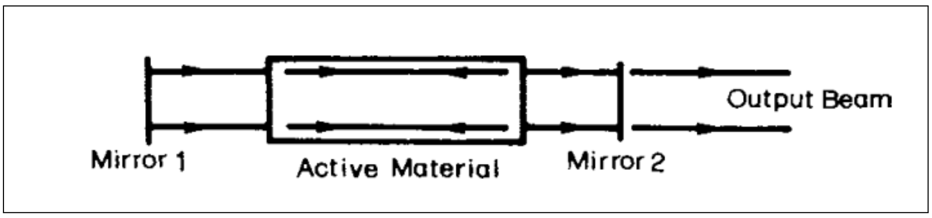

Figure III.2: **Schematic of laser**[47]

III.2.4 Coherence

Refers to the degree to which an electromagnetic wave preserves a fixed phase relationship in different points of space (spatial coherence) or over different moments in time (temporal coherence) [47]. Spatial coherence ensures a specific phase of all beam points, but temporal coherence evaluates the stability of the phase [50, 51].

III.2.5 Brightness

It is defined as the power emitted per unit of surface area per unit of solid angle (W/m^2sr). For lasers, the brightness is very high due to the small beam area and low divergence angle, It's given by [47, 51] :

$$B = \frac{4P}{(\pi D\theta)^2} \tag{III.2}$$

Where: P is the power.

The laser brightness is maximum when the beam is perfectly spatially coherent (diffraction is limited).

III.2.6 Directionality

The direction of the lasers appears when the gain medium is placed inside a resonant cavity, enforcing the nearly perpendicular waves to the mirrors (Fig. III.2) can oscillate, making the laser point in one direction [47]. In the perfect case of coherence, the beam's divergence is limited by the diffraction, which is given by:

$$\theta_d = \frac{\beta\lambda}{D} \tag{III.3}$$

Where θ_d is the diffraction angle, D is the beam diameter, β is a constant ($\approx$1), and λ is the laser wavelength.

The divergence for partial coherence increases and becomes:

$$\theta_d = \frac{\beta\lambda}{\sqrt{A_c}} \tag{III.4}$$

Where A_c is the coherence area[51, 47].

III.2.7 Repetition rate

This refers to the number of pulses emitted per second; the choice of repetition rate affects the peak power of the laser. Its generation depends on the type of laser and the mechanisms used to generate the pulses[52]. For example, the most common methods used to create laser pulses are:

1. **Mode locking:** It is a group of techniques to produce ultrafast lasers (picoseconds or femtoseconds), by locking different longitudinal modes of the laser in a laser cavity, making them oscillate simultaneously with fixed relativity, causing the modes to interfere at specific intervals, producing a periodic train of pulses. To produce higher repetition rates, a short cavity length and medium with a low refractive index must be used[53]. This relation is determined by:

$$f_{\text{rep}} = \frac{c}{2nL} \tag{III.5}$$

   Where c is the light velocity, n is the refractive index of the medium, and L is the cavity length.

2. **Q-switching:** This technique generates short light pulses, like nanosecond ones, by storing the energy of the laser pumped in a cavity with a low-quality factor (Q), using a Q-switch device. As the Q factor increases due to the Q-switch device, the stored energy is released in the form of a laser pulse (short and intense) with a duration in the nanosecond range[54].

III.2.8 Beam profile

Is the spatial distribution of light intensity, which plays a crucial role in determining the quality of laser in applications. There are many types, but in supercontinuum generation, the most common is the Gaussian beam profile, especially when using a high-quality ultrafast laser[39].

The intensity distribution of the Gaussian beam is bell-shaped, with high intensity in the center, which exponentially decreases toward the edges (Fig. III.3)[39, 55]; it is given by:

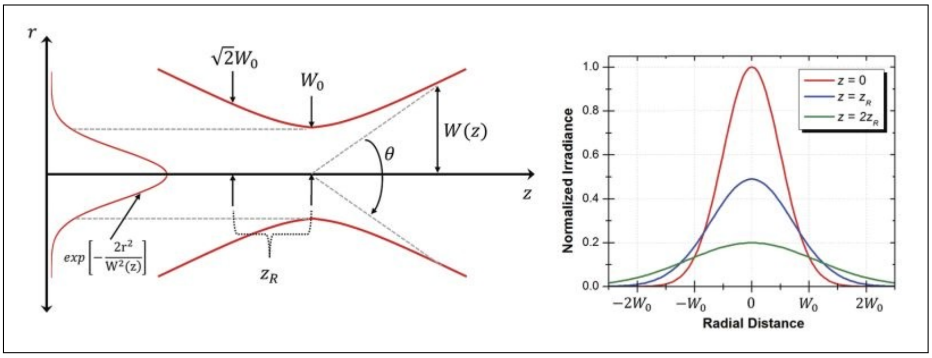

Figure III.3: **Diagram of Gaussian beam (left); the normalized irradiation of the beam as a function of the radial distance(right).**[55]

$$I(r) = I_0 \exp\left(-\frac{2r^2}{w^2(z)}\right) \tag{III.6}$$

Where:

- I_0: The peak intensity at the center of the beam.
- r: The radial distance.
- $w(z)$: The beam radius at position z

The radius position is given by:

$$W(z) = W_0\sqrt{1+\left(\frac{z}{z_R}\right)^2} \quad \text{where} \quad z_R = \frac{\pi W_0^2}{\lambda}. \tag{III.7}$$

With: z_R: represents the distance from the waist.

In this chapter, we explored the intrinsic properties of water as the nonlinear medium and the critical characteristics of lasers that influence supercontinuum generation. Understanding water's dielectric nature, high nonlinear refractive index, absorption spectrum, and dispersion behavior is essential for accurately modeling the interaction of ultrashort laser pulses within it. The optical transparency of water in the visible and near-infrared regions, combined with its dispersion properties, sets the foundation for efficient nonlinear phenomena such as self-phase modulation and self-focusing.

Additionally, the laser parameters including pulse width, peak power, wavelength, coherence, brightness, directionality, and repetition rate play a pivotal role in determining the efficiency and spectral characteristics of the generated supercontinuum. The interplay between the medium's properties and the laser source parameters governs the complex nonlinear optical processes involved.

This information lays a solid groundwork for the following chapter, where the results of supercontinuum generation experiments and simulations will be presented and analyzed in detail.

Numerical Simulation of Femtosecond Laser-Induced Supercontinuum Generation in Water: Results and Discussion

IV. Numerical Simulation of Femtosecond Laser-Induced Supercontinuum Generation in Water: Results and Discussion

This chapter presents a comprehensive numerical study of supercontinuum generation (SCG) in water induced by femtosecond laser pulses. SCG is a highly nonlinear optical phenomenon resulting in the broadening of the input pulse spectrum due to a combination of nonlinear effects such as self-phase modulation, Kerr-induced self-focusing, plasma generation, and dispersion. Water, being a weakly absorbing dielectric at 800 nm, offers a suitable medium for such nonlinear interactions. The simulations were carried out using a generalized nonlinear Schrödinger equation (GNLSE) in the frequency domain, including contributions from Kerr nonlinearity, multiphoton ionization, and plasma defocusing.

IV.1 Theoretical Model

We employed the GNLSE in the frequency domain to model the propagation of the femtosecond laser pulse in water. The equation takes into account [56]:

- Linear dispersion, characterized by the second-order dispersion coefficient $\beta_2 \approx 25\text{fs}^2/\text{mm}$ at 800 nm.
- Kerr nonlinearity, modeled by an intensity-dependent phase shift.
- Self-focusing, due to the nonlinear refractive index.
- Multiphoton ionization (MPI), a dominant ionization mechanism at 800 nm.
- Plasma formation, with inverse Bremsstrahlung absorption and defocusing effects.

$$\frac{\partial A}{\partial z} = \underbrace{-\frac{i\beta_2}{2}\frac{\partial^2 A}{\partial t^2}}_{\text{Dispersion}} + \underbrace{i\gamma|A|^2 A}_{\text{Kerr nonlinearity}} - \underbrace{\frac{\alpha}{2}A}_{\text{Linear loss}} - \underbrace{\frac{\alpha_{\mathrm{IB}}\rho_e}{2}A}_{\text{Plasma absorption}} - \underbrace{i\frac{k_0}{2n_0}\rho_e A}_{\text{Plasma defocusing}} \tag{IV.1}$$

where:

- $A = A(z,t)$: Complex pulse envelope (time domain),
- β_2: 2nd-order dispersion coefficient [$\mathrm{fs}^2/\mathrm{mm}$],
- $\gamma = \frac{n_2\omega_0}{A_{\mathrm{eff}}}$: Nonlinear parameter [$\mathrm{W}^{-1}\mathrm{m}^{-1}$]. The Effective Area A_{eff} quantifies the spatial extent of the laser beam's intensity profile. For a Gaussian beam, it is derived from the beam waist ω_0: $A_{\mathrm{eff}} = \pi\,\omega_0^2$.
- α: Linear absorption coefficient [m^{-1}].
- $\rho_e(z,t)$: Free-electron density [m^{-3}].
- α_{IB}: Inverse Bremsstrahlung absorption coefficient [m^2].
- $k_0 = \frac{2\pi}{\lambda_0}$ Wavenumber in vacuum (λ_0: central wavelength of the laser pulse in a vacuum).

Plasma Dynamics

The free-electron density evolves through multiphoton ionization (MPI) using an explicit forward Euler scheme [57]:

$$\rho_e^{(n+1)} = \rho_e^{(n)} + \Delta z \cdot \sigma_K I^{K_{\mathrm{MPI}}}(\rho_{\mathrm{nt}} - \rho_e^{(n)}) \tag{IV.2}$$

where n is the iteration index for the electron density update, $\sigma_K = 2\times10^{-21}\,\mathrm{m}^2\mathrm{s}^{-1}$, $K_{\mathrm{MPI}} = 6$, and $\rho_{\mathrm{nt}} = 6.7\times10^{28}\,\mathrm{m}^{-3}$.

Numerical Solution: Symmetrized Split-Step Fourier Method

The GNLSE is solved using a symmetrized split-step Fourier method [58]:

Step 1: Linear Step (Frequency Domain, Half-Step)

Propagate half-step using dispersion and linear absorption [58]:

$$\tilde{A}(\omega, z + \Delta z/2) = \tilde{A}(\omega, z) \exp\left[\left(D(\omega) - \frac{\alpha}{2}\right)\frac{\Delta z}{2}\right] \tag{IV.3}$$

$$D(\omega) = -\frac{i\beta_2}{2}\omega^2 \tag{IV.4}$$

where ω is the angular frequency grid for dispersion calculation in the Fourier domain.

Step 2: Nonlinear Step (Time Domain)

- Compute intensity: $I = |A|^2/A_{\text{eff}}$.
- Update plasma density via Euler method (Eq. (IV.2)).
- Apply nonlinear/plasma effects:

$$A(z + \Delta z, t) = A(z, t) \exp\left[i\gamma|A|^2\Delta z - \frac{\alpha_{\text{IB}}\rho_e\Delta z}{2} - i\frac{k_0}{2n_0}\rho_e\Delta z\right] \tag{IV.5}$$

Step 3: Linear Step (Frequency Domain, Half-Step)

Repeat Step 1 to complete the full symmetric step.

Numerical Implementation Details

- **Temporal Grid**: $N = 2^{14}$ points over $t \in [-10\tau_p, 10\tau_p]$ with $\tau_p = 140\,\text{fs}$.
- **Initial Condition**:

$$A(0, t) = \sqrt{P_{\text{peak}}} \exp\left(-\frac{t^2}{2\tau_g^2}\right), \quad \tau_g = \tau_p/1.665, \quad P_{\text{peak}} = \frac{E_p}{\sqrt{\pi}\tau_p} \tag{IV.6}$$

- **FFT/IFFT**: SciPy's ‘fft‘/‘ifft‘ for domain transitions.

IV.2 Simulation Parameters

Table IV.1 presents the key parameters used in our model.

Table IV.1: **Laser and water parameters used for SCG simulation**

Category	Parameter	Value	Unit
Laser Parameters			
	Wavelength (λ)	800	nm
	Pulse duration (FWHM) (τ_p)	140	fs
	Pulse energy (E)	1	μJ
	Spatial beam waist (w_0)	5	μm
	Beam propagation distance	1	cm
	Temporal profile	Gaussian	–
Water Parameters			
	Linear refractive index (n)	1.33	–
	Nonlinear refractive index (n_2)	8×10^{-20}	m^2/W
	Absorption coefficient at 800 nm	$\sim 10^{-4}$	cm^{-1}
	Ionization threshold	6.5	eV

IV.3 Initial Laser Pulse

IV.3.1 Temporal Profile

The initial laser pulse temporal profile is visualized in Figure IV.1

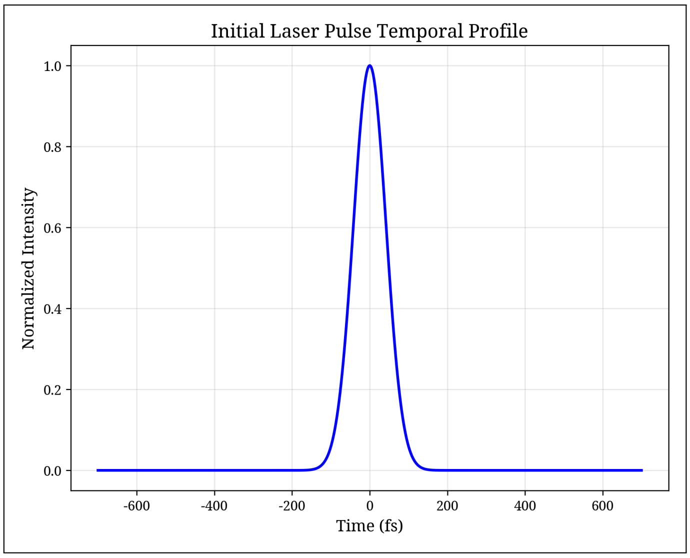

Figure IV.1: **Initial Laser Pulse Temporal Profile.**

The initial laser pulse used in our simulations has a Gaussian temporal profile with a full width at half maximum (FWHM) of approximately 140 fs, centered at t = 0 fs. This profile is typical for femtosecond Ti:Sapphire laser systems commonly used in ultrafast optics experiments. The smooth Gaussian shape indicates a transform-limited pulse with minimal chirp, which is ideal for studying nonlinear optical effects.

This choice of pulse parameters aligns with experimental setups reported by Brodeur and Chin [59], who used similar pulse durations in their studies on supercontinuum generation in condensed media.

IV.3.2 Pulse Spectrum

Figure IV.2 shows that the initial laser pulse spectrum has a bandwidth centered at 800 nm, the standard wavelength for Ti:Sapphire laser systems. Its spectral width matches that of a transform-limited 140 fs pulse. This narrow starting spectrum provides a clear baseline for observing the spectral broadening that occurs during supercontinuum generation.

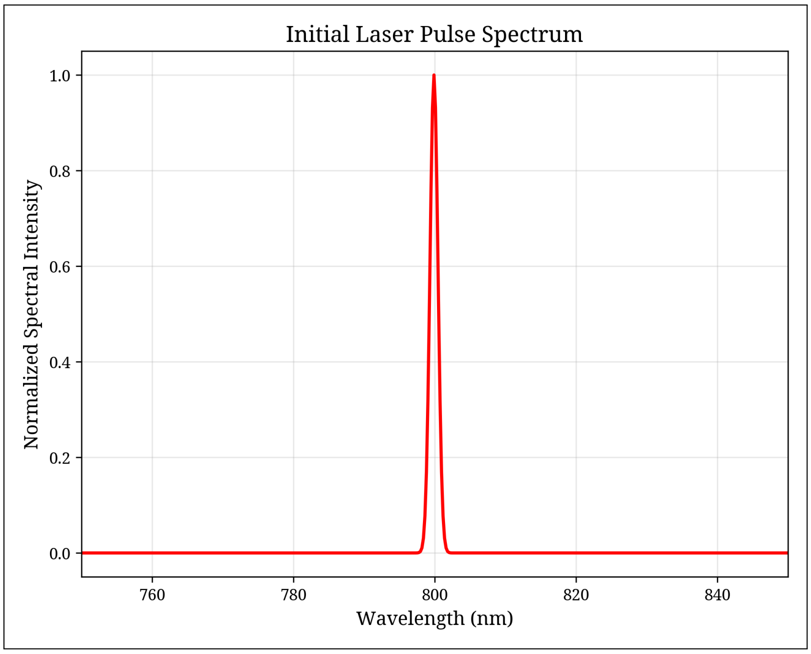

Figure IV.2: Initial Laser Pulse Spectrum

This spectral characteristic is similar to those used in experimental studies by Liu et al. [60], who employed 800 nm pulses from Ti: Sapphire lasers to investigate supercontinuum generation in water. The narrow initial bandwidth allows for precise tracking of the spectral evolution during propagation.

IV.4 Supercontinuum Spectrum Evolution

Figure IV.3 presents the evolution of the laser pulse spectrum as it propagates through the water medium. The normalized spectral intensity is plotted against wavelength for different normalized propagation distances: the initial pulse ($z/z_{max} = 0$, blue line) and at subsequent points $z/z_{max} = 0.3$ (orange), $z/z_{max} = 0.6$ (green), and $z/z_{max} = 1.0$ (red).

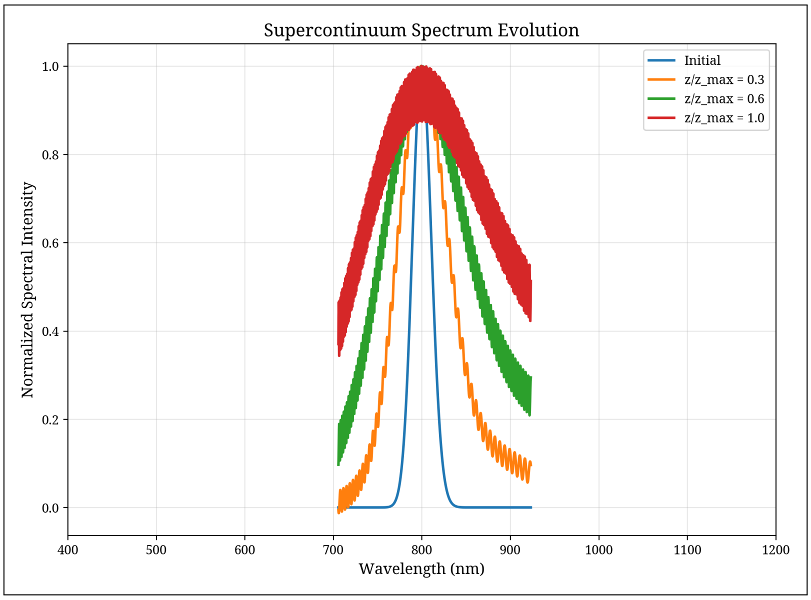

Figure IV.3: Supercontinuum spectrum evolution.

The input laser pulse possesses a narrow spectrum centered around the fundamental wavelength of 800 nm (characteristic of the initial femtosecond pulse before significant nonlinear interaction). As the pulse propagates, its spectrum undergoes important broadening. At $z/z_{max} = 0.3$, noticeable broadening occurs, primarily towards longer wavelengths (red-shift). By $z/z_{max} = 0.6$, the broadening is substantial, extending significantly to both shorter (blue-shift) and longer wavelengths compared to the initial spectrum. At the final propagation distance ($z/z_{max} = 1.0$), the spectrum spans a vast range, from below 700 nm to beyond 950 nm, signifying the generation of a broad supercontinuum.

The observed spectral broadening is driven predominantly by self-phase modulation (SPM). SPM arises from the time-dependent nonlinear phase shift imparted on the pulse due to the intensity-dependent refractive index (Kerr effect) and the rapidly changing refractive index associated with plasma generation.

The broadened spectrum at $z/z_{max} = 1.0$ exhibits some asymmetry, with potentially more pronounced broadening towards the red side initially, although significant blue-shifting also occurs. This asymmetry can be influenced by self-steepening effects, plasma-induced blue-shifting, and the specific dispersion profile of water. Furthermore, the spectrum displays pronounced oscillatory structures (modulations). These modulations are characteristic of SPM and can arise from the interference between different frequency components generated at different temporal parts of the pulse or potentially indicate temporal pulse splitting followed by interference. The extent of spectral broadening directly correlates with the propagation distance, consistent with the cumulative nature of nonlinear phase accumulation.

IV.5 Phase Diagram for Supercontinuum Generation

The figure IV.4 presents a phase diagram illustrating the dependence of supercontinuum generation (SCG) efficiency, quantified by the normalized spectral width, on the input laser pulse duration (femtoseconds) and the normalized input power (P/P_{cr}). P_{cr} represents the critical power for self-focusing, a key threshold parameter in nonlinear optics. The color map, ranging from deep purple (low spectral width) to bright yellow (high spectral width), provides a quantitative visualization of the SCG extent across the parameter space.

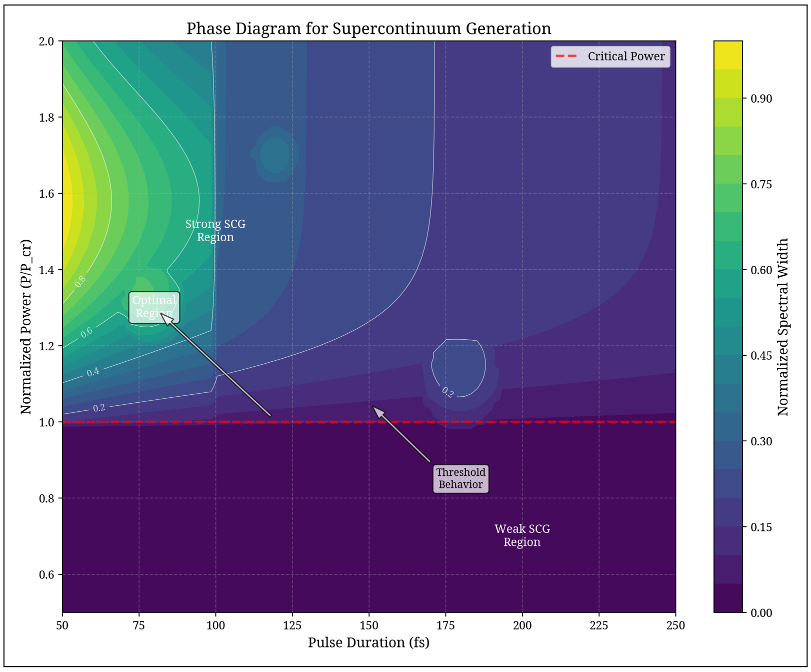

Figure IV.4: Phase diagram for SCG.

The diagram prominently features a dashed red line at $P/P_{cr} = 1$, explicitly demarcating the critical power threshold. Below this threshold ($P/P_{cr} < 1$), the normalized spectral width remains minimal, indicating negligible or weak SCG. This region is appropriately labeled as the "Weak SCG Region". This observation underscores the fundamental role of self-focusing, which only becomes dominant when the input power exceeds the critical power, in initiating significant spectral broadening.

Above the critical power threshold ($P/P_{cr} > 1$), a dramatic increase in the normalized spectral width is observed, signifying the onset of efficient SCG. This area is designated as the ”Strong SCG Region”. The spectral broadening is a direct consequence of enhanced self-phase modulation (SPM) and other nonlinear processes, which are significantly amplified once self-focusing overcomes diffraction.

Within the strong SCG regime, the diagram reveals an ”Optimal Region” where the spectral broadening reaches its maximum extent (indicated by the brightest yellow/green colors and contours corresponding to high spectral width values, e.g., > 0.8). This optimal window appears centered around pulse durations of approximately 80-100 fs and normalized powers of $P/P_{cr} \approx 1.2 - 1.4$. This suggests a complex interplay between pulse duration, peak power, and the dynamics of self-focusing, plasma generation, and dispersion, leading to an optimal condition for maximizing spectral bandwidth.

For a fixed power above P_{cr}, the spectral width generally decreases as the pulse duration increases beyond the optimal region (e.g., towards 250 fs). This can be attributed to factors such as the inverse relationship between initial peak intensity and pulse duration for a fixed energy, and potentially stronger group velocity dispersion effects for longer pulses which might limit the interaction length or efficiency of temporal compression mechanisms.

The arrow labeled ”Threshold Behavior” points towards the transition zone around $P/P_{cr} = 1$, emphasizing the sharp change in SCG efficiency as the input power crosses this critical value. This highlights the highly nonlinear nature of the SCG process and its strong dependence on reaching sufficient intensity for self-focusing to dominate.

This phase diagram (IV.4 provides a valuable map for predicting and optimizing SCG in water. The simulation parameters provided in IV.1 ($\tau_p = 140$ fs, $P/P_{cr} > 1$) fall within the ”Strong SCG Region”, consistent with the significant spectral broadening observed in figure IV.3. The diagram effectively encapsulates the critical dependence of SCG on exceeding the self-focusing threshold and identifies the parameter space conducive to efficient broadband light generation.

IV.6 Spatiotemporal Intensity Evolution

Figure IV.5 provides a three-dimensional visualization of the laser pulse intensity evolution, mapping normalized intensity (represented by color and height) as a function of both propagation distance ($z-$axis, 0 to 1.0 cm) and local time within the pulse frame ($t-$axis, -800 to 800 fs). This spatio-temporal representation offers insights into how the pulse shape and peak intensity change dynamically during propagation.

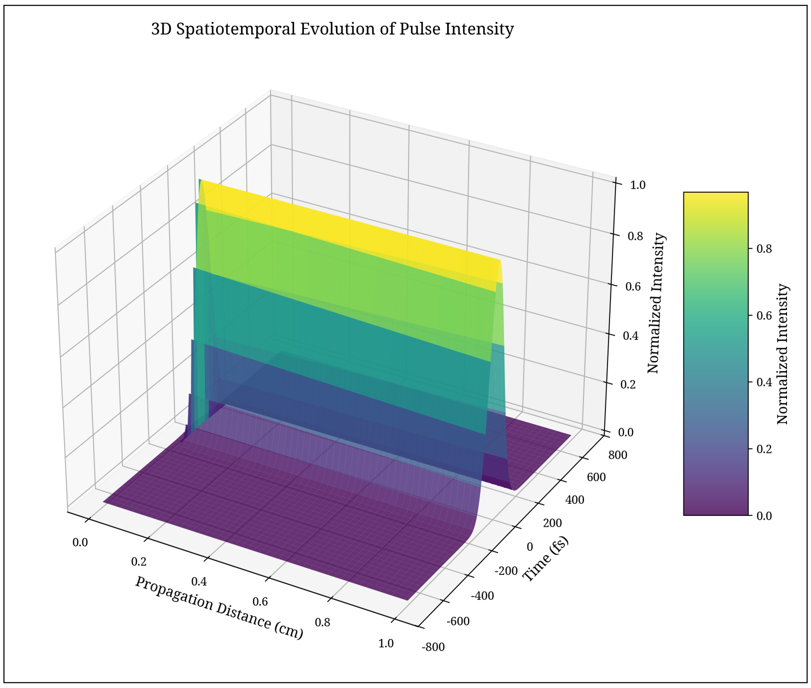

Figure IV.5: **Spatiotemporal Intensity Evolution.**

Figure IV.5 clearly shows an increase in the peak normalized intensity as the pulse propagates from z=0 towards z=1.0 cm. This is consistent with the self-focusing phenomenon, where the beam spatially contracts, leading to higher on-axis intensity.

While the initial pulse likely has a smooth temporal profile (Gaussian), the figure suggests modifications to this profile during propagation. The intensity distribution appears to become steeper at the leading edge and potentially develops substructures or undergoes compression/broadening, although the resolution might limit detailed observation.

The highest intensities are confined to the central temporal region of the pulse (around t=0 fs) and occur at longer propagation distances where self-focusing effects are most pronounced. This spatio-temporal localization is critical for driving highly nonlinear processes like MPI and strong SPM.

Figure IV.5 serves as a comprehensive qualitative overview, integrating the spatial focusing aspect (implicitly, via intensity increase) with the temporal evolution. It visually confirms that the conditions for strong nonlinear interactions (high intensity) are met and sustained over a significant portion of the propagation path, particularly in the latter stages.

IV.7 Spatial Beam Profile Evolution

Figure IV.6 visualizes the evolution of the laser beam's spatial intensity profile as it propagates through the medium. It plots the normalized intensity (color map and height) against the radial distance from the beam axis ($x-$axis, 0 to 20 μm) and the propagation distance ($y-$axis, 0 to 1.0 cm).

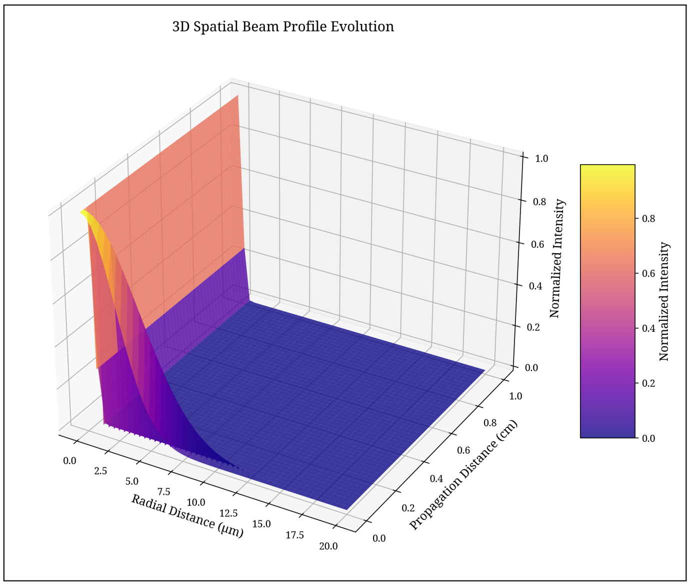

Figure IV.6: **Spatial beam profile.**

At the entrance of the medium (z=0), the beam exhibits a Gaussian profile, with a characteristic width (initial waist $w_0 = 5$ μm. As the beam propagates along the $z-$axis, an important reduction in its radial extent is observed. The high-intensity core of the beam contracts significantly, concentrating the energy towards the propagation axis (r=0). This spatial collapse is a direct visualization of the self-focusing effect driven by the Kerr nonlinearity for $P > P_{cr}$.

While strong focusing is evident, the beam does not appear to collapse to an infinitesimal point (singularity). Instead, the minimum beam waist seems to stabilize or be arrested at a finite value at longer propagation distances. This arrest of self-focusing is typically attributed to counteracting effects, most notably plasma defocusing, which becomes significant at the high intensities reached near the focus.

The plot (figure IV.6) clearly shows that the highest intensities are tightly confined to a small radial region near the axis ($r \approx 0$) after propagating some distance, confirming the spatial localization of the intense light required for efficient nonlinear interactions.

IV.8 Supercontinuum Spectral Evolution

Figure IV.7 shows a three-dimensional perspective on the spectral evolution during supercontinuum generation. It plots the normalized spectral intensity (color map and height) as a function of wavelength ($x-$axis, 400 to 1200 nm) and propagation distance ($y-$axis, 0 to 1.0 cm).

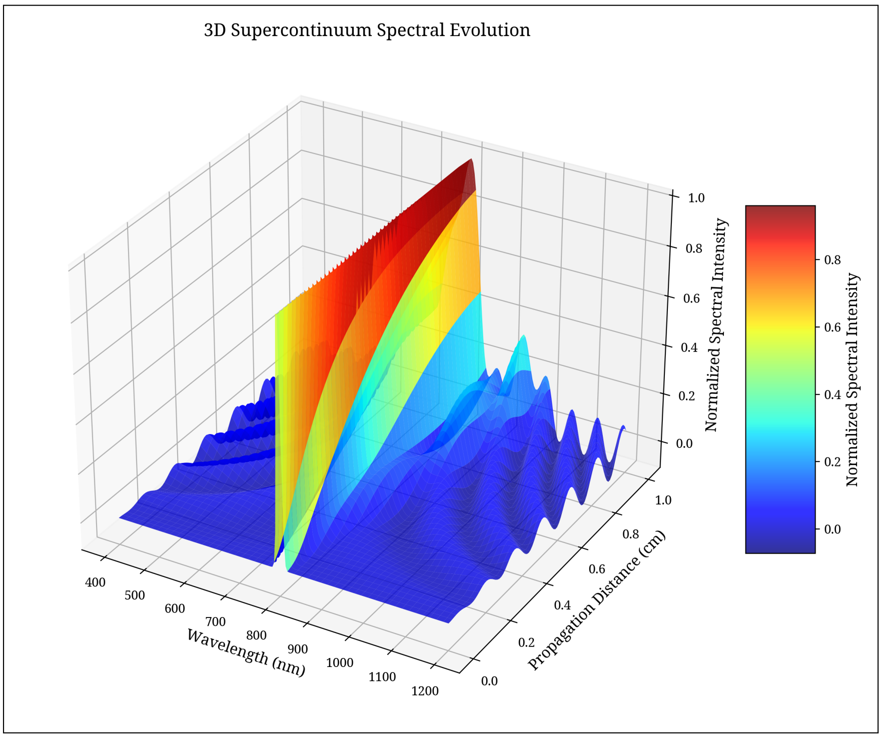

Figure IV.7: **Supercontinuum Spectral Evolution.**

Figure IV.7 illustrates the progressive broadening of the spectrum as the pulse propagates through the water medium. Starting from a narrow spectral peak centered at 800 nm at z=0, the spectrum expands dramatically along the propagation axis. At the output (z=1.0 cm), the spectrum covers a wide range, extending from the visible (below 700 nm) into the near-infrared (beyond 1100 nm), characteristic of a well-developed supercontinuum.

The three-dimensional view reveals the dynamic nature of the spectral broadening process. New frequency components appear and intensify at different propagation distances. The complex structure, including the emergence of distinct spectral peaks and valleys, evolves continuously along the $z-$axis.

The broadening mechanism, primarily SPM, is clearly visualized as the spectral energy spreads out from the initial 800 nm peak with increasing propagation distance. The generation of frequencies both lower (red-shifted) and higher (blue-shifted) than the input frequency is evident.

IV.9 Plasma Density Distribution

Figure IV.8 presents a three-dimensional visualization of the generated plasma density. It maps the normalized plasma density (color map and height) as a function of radial distance ($x-$axis, 0 to 20 μm) and local time within the pulse frame ($y-$axis, -800 to 800 fs). This likely represents the plasma distribution at a specific, advanced propagation distance (e.g. z=1.0 cm) where plasma generation is significant.

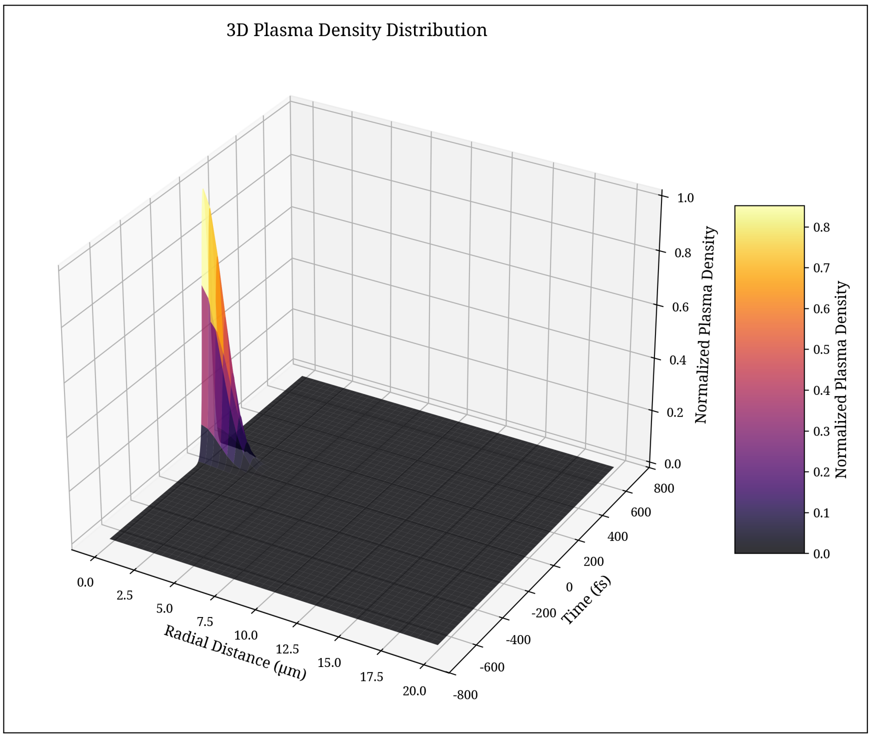

Figure IV.8: **3D visualization of plasma density distribution in space and time.**

The plasma is highly localized both spatially and temporally. Spatially, the highest plasma density is confined to the central region of the beam (small radial distances, $r \approx 0$). Temporally, it is concentrated around the peak of the pulse ($t \approx 0$ fs). This spatio-temporal distribution directly mirrors the region of highest laser intensity, as expected from the intensity-dependent nature of multiphoton ionization (MPI). The plasma forms preferentially where and when the laser intensity exceeds the ionization threshold. This confirms the tight coupling between the intensity dynamics (governed by self-focusing, see figure IV.5 and IV.6) and the plasma generation process.

The plasma density exhibits relatively sharp boundaries in both the radial and temporal dimensions, reflecting the highly nonlinear dependence of MPI rates on laser intensity. Below the threshold intensity, ionization is negligible.

Figure IV.8 provides a detailed spatio-temporal map of the plasma generated during SCG. Understanding this distribution is crucial because the plasma significantly influences the pulse propagation through plasma defocusing (affecting the refractive index) and absorption. The localized nature of the plasma ensures that its effects are most pronounced on the highest intensity part of the pulse, contributing to complex reshaping dynamics and influencing the spectral broadening process (e.g., via plasma-induced blue-shifting and phase modulation).

IV.10 Parameter Space for Supercontinuum Generation

Figure IV.9 presents a three-dimensional surface plot visualizing the normalized spectral width (representing SCG efficiency) as a function of normalized input power (P/P_{cr}, $x-$axis, 0.4 to 2.0) and input pulse duration ($y-$axis, 50 to 250 fs). The normalized spectral width is represented by the height of the surface and the color map.

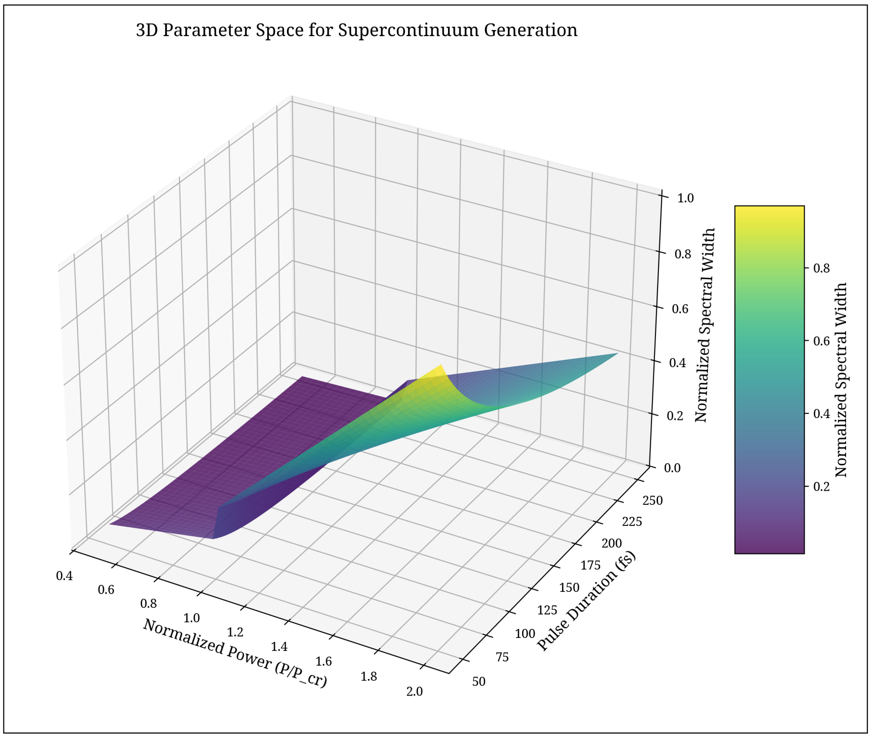

Figure IV.9: **3D parameter space for SCG.**

Figure IV.9 clearly illustrates the threshold behavior around $P/P_{cr} = 1$. For $P/P_{cr} < 1$, the surface remains flat and low (dark purple), indicating minimal spectral broadening regardless of pulse duration. As P/P_{cr} increases beyond 1, the surface rises steeply, signifying the onset of efficient SCG.

This plot (IV.9) effectively combines the dependencies shown in the 2D phase diagram (figure IV.4) into a single surface. It confirms that achieving significant spectral broadening requires exceeding the critical power threshold. Furthermore, it visualizes how, for a given supercritical power ($P/P_{cr} > 1$), the efficiency of SCG varies with pulse duration, generally showing an optimal duration range (around 75-125 fs in this view) where the spectral width is maximized.

The surface exhibits a ridge corresponding to the optimal conditions for SCG, where the spectral width reaches its peak. This ridge is located in the $P/P_{cr} > 1$ region and appears to curve slightly within the pulse duration axis, consistent with the ”Optimal Region” identified in the 2D phase diagram (figure IV.4).

In this chapter, we presented a detailed numerical investigation of SCG in water under femtosecond laser excitation. We modeled the complex interplay of nonlinear effects involved in SCG by solving the GNLS equation that describes these terms. Our simulations confirm that:

- Water is an effective nonlinear medium for SCG.
- The Spectral Broadening is asymmetric, extending from 700nm (blue-shifted), which is influenced by plasma effects, to above 1100nm (red-shifted), shaped by self-phase modulation (SPM) and the self-steepening.
- The spatiotemporal intensity profile shows a strong self-focusing effect, where the pulse collapses in the transverse direction and compresses temporally, leading to intensity peaks that trigger multiphoton ionization.
- Plasma density is highly localized at the spatiotemporal center of the pulse, both radially ($r \approx 0$) and temporally ($t \approx 0$ fs), coinciding with the region of maximum intensity. This supports the expected intensity dependence of multiphoton ionization.
- A clear power threshold exists at $P/P_{cr} \approx 1$, beyond which SCG becomes efficient. Below this threshold, spectral broadening is minimal regardless of pulse duration.
- The parameter space analysis reveals an optimal regime for SCG in the pulse duration range of 75–125 fs, where the balance between peak power and nonlinear interaction is maximized. The longer durations lead to reduced efficiency while too short durations (<70 fs) may result in stronger plasma effects that limit spectral extension.

These results will guide innovative experimental setups and future applications of SCG in various fields.

Conclusion

conclusion

This study has offered a comprehensive numerical framework and theoretical investigation of supercontinuum generation (SCG) in water, initiated by femtosecond laser pulses, and simulated by solving the Generalized Nonlinear Schrodinger Equation (GNLSE).

From a theoretical standpoint, the work first confirmed the pertinence of water as a nonlinear medium, highlighting its unique properties that affect the generation of the supercontinuum. The dominant nonlinear effects involved in the process (e.g. Kerr effect, Self-phase modulation, filamentation…) were studied in detail to build a coherent understanding of their contributions to the evolution of the broad spectrum.

On the practical side, the numerical simulations demonstrated that femtosecond laser pulses at 800 nm, with a FWHM around 140 fs, and energies in the microjoule range, are capable of generating a broad and asymmetric supercontinuum in water. The spectral broadening observed from approximately 700 nm to beyond 1100 nm was shown to result from the action of SPM, plasma effects, and other nonlinear effects in this medium.

The results confirmed the existence of a critical input power threshold ($P/Pc \approx 1$) necessary for efficient SCG. Below this threshold, the nonlinear effects are weak, which means that the spectral broadening is negligible. However, as the input power exceeds this threshold, the propagation dynamics are dominated by strong nonlinearities, enabling significant spectral broadening. An optimal regime of SCG was observed within a pulse duration range of 80-100 fs and a normalized input power of $P/P_{cr} \approx 1.2 - 1.4$. This regime achieves a favorable balance between peak intensity and nonlinear interaction, while avoiding excessive plasma generation that could otherwise limit the spectral broadening.

The special and temporal evolution of the laser pulse profiles with the density distribution confirmed the role of strong self-focusing followed by localized plasma formation. These effects are crucial in shaping the final continuum. In conclusion, the results of this thesis contribute to a deeper understanding of SCG in aqueous media and offer clear guidance for optimizing laser parameters to achieve an optimal broad and stable continuum in water. These perspectives obtained here are crucial to support future design setups and enhance the development of supercontinuum sources for applications in biomedical imaging, spectroscopy, and other domains necessitating broadband coherent light.

Bibliography

Bibliography

[1] John Michael Dudley and Goëry Genty. Supercontinuum light. *Physics Today*, 66:29–34, 2013.

[2] Than Singh Saini and Ravindra Kumar Sinha. Mid-infrared supercontinuum generation in soft-glass specialty optical fibers: A review. *Progress in Quantum Electronics*, 78:100342, 2021.

[3] Truong X Tran and Fabio Biancalana. Dynamics and control of the early stage of supercontinuum generation in submicron-core optical fibers. *Physical Review A—Atomic, Molecular, and Optical Physics*, 79(6):065802, 2009.

[4] BP Stoicheff. Characteristics of stimulated raman radiation generated by coherent light. *Physics Letters*, 7(3):186–188, 1963.

[5] RR Alfano and SL Shapiro. Emission in the region 4000 to 7000 å via four-photon coupling in glass. *Physical Review Letters*, 24(11):584, 1970.

[6] Linley Li Lin, Xinyuan Bi, Yuqing Gu, Fu Wang, and Jian Ye. Surface-enhanced raman scattering nanotags for bioimaging. *Journal of Applied Physics*, 129:191101, 04 2021.

[7] Y Fujii, Brian S Kawasaki, Kenneth O Hill, and Derwyn C Johnson. Sum-frequency light generation in optical fibers. *Optics letters*, 5(2):48–50, 1980.

[8] K Washio, K Inoue, and T Tanigawa. Efficient generation of near-ir stimulated light scattering in optical fibres pumped in low-dispersion region at 1.3 μm. *Electronics Letters*, 16(9):331–333, 1980.

[9] Barry Gross and Jamal T Manassah. Supercontinuum in the anomalous group-velocity dispersion region. *Journal of the Optical Society of America B*, 9(10):1813–1818, 1992.

[10] Kunihiko Mori, T Morioka, and M Saruwatari. Ultrawide spectral range group-velocity dispersion measurement utilizing supercontinuum in an optical fiber pumped by a 1.5/spl mu/m compact laser source. *IEEE Transactions on Instrumentation and Measurement*, 44(3):712–715, 1995.

[11] JC Knight, TA Birks, P St J Russell, and DM Atkin. All-silica single-mode optical fiber with photonic crystal cladding. *Optics letters*, 21(19):1547–1549, 1996.

[12] Mikko Lehtonen, Goery Genty, Hanne Ludvigsen, and Matti Kaivola. Supercontinuum generation in a highly birefringent microstructured fiber. *Applied physics letters*, 82(14):2197–2199, 2003.

[13] AV Husakou and J Herrmann. Supercontinuum generation of higher-order solitons by fission in photonic crystal fibers. *Physical review letters*, 87(20):203901, 2001.

[14] Amine Salem, Rim Cherif, and Mourad Zghal. Nonlinear fiber optics: Application to supercontinuum generation. *Springer Proceedings in Physics*, 166:37–46, 2015.

[15] Sven E Fiedler, Gerald Hoheisel, Albert A Ruth, and Achim Hese. Incoherent broadband cavity-enhanced absorption spectroscopy of azulene in a supersonic jet. *Chemical physics letters*, 382(3-4):447–453, 2003.

[16] Chetan Poudel and Clemens F Kaminski. Supercontinuum radiation in fluorescence microscopy and biomedical imaging applications. *Journal of the Optical Society of America B*, 36(2):A139–A153, 2019.

[17] M. K. Lu, H. Y. Lin, C. C. Hsieh, and F. J. Kao. Supercontinuum as a light source for miniaturized endoscopes. *Biomedical Optics Express*, 7(9):3335–3342, 2016.

[18] Rüdiger Paschotta. Optical fiber communications, 2025. Accessed: 14 March 2025.

[19] Leif Katsuo Oxenløwe. Optical frequency combs for optical fiber communications. *APL Photonics*, 10(1), 2025.

[20] M. Centini. Introduction to non linear optics. In *Preparatory School to the Winter College on Fibre Optics, Fibre Lasers and Sensors*, Roma, Italy, 2007. Universita' di Roma, "La Sapienza".

[21] Michelle Moreno. Kerr effect. *Instituto de Física de São Carlos, Universidade de São Paulo*, June 2018.

[22] Rüdiger Paschotta. Self-phase modulation, 2025. Accessed: 2025-03-24.

[23] Nitu Borgohain and Swapan Konar. Self-phase modulation dominated supercontinuum generation employing cosh-gaussian pulses in photonic crystal fibers. *Journal of Nanophotonics*, 9:093098, 2015.

[24] Arnaud Couairon and André Mysyrowicz. Femtosecond filamentation in transparent media. *Physics reports*, 441(2-4):47–189, 2007.

[25] COMSOL Multiphysics. Self-focusing. `https://www.comsol.com`, 2025. Created in COMSOL Multiphysics 5.6.

[26] Gadi Fibich and Alexander L Gaeta. Critical power for self-focusing in bulk media and in hollow waveguides. *Optics letters*, 25(5):335–337, 2000.

[27] F. V. Potemkin, E. I. Mareev, and E. O. Smetanina. Influence of wave-front curvature on supercontinuum energy during filamentation of femtosecond laser pulses in water. *Physical Review A*, 97(3):033801, 2018.

[28] Sergey Mitryukovskiy. *Coherent Secondary Radiation from Femtosecond Laser Filaments*. Theses, École Polytechnique, September 2014.

[29] Thomas H. Kauffmann, Ninel Kokanyan, and Marc D. Fontana. Use of stokes and anti-stokes raman scattering for new applications. *Journal of Raman Spectroscopy*, 50(3):418–424, 2019.

[30] Pau Arcos, Arturo Mena, María Sánchez-Hernández, Eneko Arrospide, Gotzon Aldabaldetreku, María Asunción Illarramendi, Joseba Zubia, and David Novoa. Narrowband stimulated raman scattering and molecular modulation in anti-resonant hollow-core fibres. *Europhysics Letters*, 147(4):45001, 2024.

[31] Robin R. Jones, David C. Hooper, Liwu Zhang, Daniel Wolverson, and Ventsislav K. Valev. Raman techniques: Fundamentals and frontiers. *Nanoscale Research Letters*, 14(231):1–34, 2019.

[32] Martin Chaplin. Complex dielectric constant of water. `https://water.lsbu.ac.uk/water/complex_dielectric.html`, 2021. Accessed: 2025-04-24.

[33] R. Paschotta. Nonlinear index, 2006.

[34] Ilyes Betka. Nonlinear optical refractive index measurements of pure water via z-scan technique at 800 nm. *arXiv preprint arXiv:2502.02944*, 2025.

[35] Christopher Baird. Absorption of electromagnetic radiation. *AccessScience*, 2025.

[36] George Hale and Marvin Querry. Optical constants of water in the 200-nm to 200-μm wavelength region. *Applied Optics*, 12:555–563, 03 1973.

[37] John M. Dudley, Goëry Genty, and Stéphane Coen. Supercontinuum generation in photonic crystal fiber. *Rev. Mod. Phys.*, 78:1135–1184, Oct 2006.

[38] J. A. Dharmadhikari, G. Steinmeyer, G. Gopakumar, D. Mathur, and A. K. Dharmadhikari. Femtosecond supercontinuum generation in water in the vicinity of absorption bands. *Optics Letters*, 41(15):3475–3478, 2016.

[39] Bahaa E. A. Saleh and Malvin Carl Teich. *Fundamentals of Photonics*. Wiley Series in Pure and Applied Optics. Wiley, Hoboken, NJ, 3rd edition, 2019.

[40] Curtis D. Mobley. Anomalous dispersion. `https://www.oceanopticsbook.info/view/theory-electromagnetism/level-2/anomalous-dispersion`, 2021. Accessed: 2025-04-21.

[41] R. Paschotta. Chromatic dispersion. RP Photonics Encyclopedia, 2005. Available online at `https://www.rp-photonics.com/chromatic_dispersion.html`.

[42] Masahiko Daimon and Akira Masumura. Measurement of the refractive index of distilled water from the near-infrared region to the ultraviolet region. *Applied Optics*, 46(18):3811–3820, 2007.

[43] David J Segelstein. *The complex refractive index of water*. PhD thesis, University of Missouri–Kansas City, 1981.

[44] Mehmet Hancer, Roger P Sperline, and Jan D Miller. Anomalous dispersion effects in the ir-atr spectroscopy of water. *Applied spectroscopy*, 54(1):138–143, 2000.

[45] B. Stuart. *Infrared Spectroscopy: Fundamentals and Applications*. Wiley, Chichester, UK, 2004.

[46] Guoqiang Lan, Yachen Gao, and Xueru Zhang. Measurement of chromatic dispersion of liquid in a wide spectral range based on liquid-prism surface plasmon resonance sensor. *Sensing and bio-sensing research*, 16:32–36, 2017.

[47] Orazio Svelto. *Principles of Lasers*. Springer, 5th edition, 2010.

[48] Govind P. Agrawal. *Nonlinear Fiber Optics*. Academic Press, Amsterdam; Boston; Heidelberg; London; New York; Oxford; Paris; San Diego; San Francisco; Singapore; Sydney; Tokyo, 5th edition, 2013.

[49] Steven L Jacques. Corrigendum: Optical properties of biological tissues: a review. *Physics in Medicine & Biology*, 58(14):5007–5008, 2013.

[50] R. Paschotta. Coherence, 2007.

[51] Narendra Kumar Pandey. Properties of laser beams. *Department of Physics, University of Lucknow*, 2025. Email: profnarendrapandey137@gmail.com.

[52] R. Paschotta. Pulse repetition rate. RP Photonics Encyclopedia, 2005.

[53] R. Paschotta. Mode locking. RP Photonics Encyclopedia, 2005.

[54] R. Paschotta. Q switching.

[55] Newport Corporation. Laser beam characterization. `https://www.newport.com/n/laser-beam-characterization`. Accessed: 2025-04-25.

[56] K. Hosseini, F. Alizadeh, E. Hinçal, B. Kaymakamzade, K. Dehingia, and M. S. Osman. A generalized nonlinear schrödinger equation with logarithmic nonlinearity and its gaussian solitary wave. *Optical and Quantum Electronics*, 56(4), 2024. Accessed: 2025-05-06.

[57] J. Noack and A. Vogel. Laser-induced plasma formation in water at nanosecond to femtosecond time scales: Calculation of thresholds, absorption coefficients, and energy density. *IEEE Journal of Quantum Electron*, 35(8):1156–1167, 1999.

[58] F. St-Hilaire. *Numerical Modeling of Supercontinuum Generation in Optical Fibers*. Master of Engineering, McGill University, 2020.

[59] A. Brodeur and S. L. Chin. Ultrafast white-light continuum generation and self-focusing in transparent condensed media. *J. Opt. Soc. Am. B*, 16:637–650, 1999.

[60] W. Liu, O. Kosareva, I. S. Golubtsov, A. Iwasaki, A. Becker, V. P. Kandidov, and S. L. Chin. Femtosecond laser pulse filamentation versus optical breakdown in h_2o. *Applied Physics B*, 76:215–229, 2003.

Abstract

This thesis investigates supercontinuum generation (SCG) in water using femtosecond laser pulses. By solving the Generalized Nonlinear Schrödinger Equation and simulating laser pulse evolution, the results confirm water as an efficient SC medium due to its high refractive index and transparency. A threshold behavior near critical power (1.2–1.4) and an optimal pulse duration (75–125 fs) were found to maximize spectral broadening. Key nonlinear effects include plasma reshaping, self-phase modulation (SPM), and self-focusing (SF), all contributing to spectrum expansion.

Keywords: Supercontinuum Generation – Femtosecond Pulses – Water – Nonlinear Effects – GNLSE – Spectral Broadening.

Résumé

Cette thèse étudie la génération de supercontinuum (SCG) dans l'eau à l'aide de lasers femtosecondes. En résolvant l'équation généralisée de Schrödinger et en simulant l'évolution des impulsions, les résultats montrent que l'eau est un milieu efficace grâce à son indice de réfraction élevé et sa transparence. Un comportement de seuil entre 1.2 et 1.4 et une durée d'impulsion optimale (75–125 fs) maximisent l'élargissement spectral. Les effets non linéaires clés incluent les effets de plasma, la modulation de phase auto-induite (SPM), et l'auto-focalisation (SF).

Mots clés : Génération de Supercontinuum – Impulsions Femtosecondes – Eau – Effets Non Linéaires – Équation GNLSE – Élargissement Spectral.

مُلخّص:

تتناول هذه الدّراسة توليد الطّيف المتّصل في الماء باستخدام نبضات ليزر فامتوثانية. أظهرت النّتائج بعد حلّ المعادلة العامّة غير الخطيّة لشرودينجر، أنّ الماء وسط فعّال لتوليد الطّيف بسبب ارتفاع معامل الانكسار وشفافيّته. لوحظ سلوك عتبة بالقرب من القدرة الحرجة (1.2–1.4) وزمن نبضة مثاليّ (75–125 فمتوثانية) يحقّق أقصى توسّع طيفيّ. تشمل التّأثيرات غير الخطيّة الرئيسيّة تأثيرات البلازما، التّعديل الذاتي للطّور(SPM) ، والتّركيز الذاتي(SF) .

الكلمات المفتاحية: توليد الطّيف المتّصل – نبضات فامتوثانية – الماء – تأثيرات غير خطيّة – المعادلة غير الخطيّة لشرودينجر – التوسّع الطّيفي.